Modelling Heat Transfer and Pathogen Disinfection in a Biogas-Powered Self-Sanitizing Toilet

by

Lilya S. Ouksel

Department of Civil and Environmental Engineering
Duke University

Date:_____

Approved:

_____
Marc Deshusses, Supervisor

_____
Mark Wiesner

_____
Claudia Gunsch

_____
Marc Jeuland

Thesis submitted in partial fulfillment of
the requirements for the degree of
Master of Science in the Department of
Civil and Environmental Engineering in the Graduate School
of Duke University
2014

ABSTRACT

Modelling Heat Transfer and Pathogen Disinfection in a Biogas-Powered Self-Sanitizing Toilet

by

Lilya Ouksel

Department of Civil and Environmental Engineering
Duke University

Date:_____

Approved:

_____
Marc Deshusses, Supervisor

_____
Mark Wiesner

_____
Claudia Gunsch

_____
Marc Jeuland

An abstract of a thesis submitted in partial
fulfilment of the requirements for the degree
of Master of Science in the Department of
Civil and Environmental Engineering in the Graduate School of
Duke University
2014

Abstract

The problem of inadequate sanitation in less developed countries has dire health consequences such as diarrheal diseases. A household-scale sanitation system consisting of an anaerobic digester, heat exchanger, and biogas-powered heater, was developed to provide a simple, potentially low cost and low carbon-footprint solution to this problem. A conceptual model was developed to predict the effectiveness of the heat sterilization system in reaching the appropriate temperatures to significantly inactivate pathogens such as *E. coli*, helminthe ova, and viruses. Lab experiments with a stainless steel heater and exchanger were used to establish model parameters and to verify the model. Though the model sometimes predicts higher or lower values than the experimental data, probably due to uncertainties in pathogen decay constants and in the different heat transfer coefficients, the model adequately predicts temperature across the heat exchanger and heater, and can provide a preliminary estimate of pathogen inactivation within the system. Both disinfection experiments showed the system reduces *E. coli* concentrations to below the WHO limit, which was predicted by the model.

Contents

List of Tables

List of Figures

List of Equations

Acknowledgements

I'd like to thank my advisor, Dr. Marc Deshusses, for his infinite patience with me as I struggled through the world of research. That combined with his high expectations and attention to detail are the only reason this thesis is complete.

The bio-engineers in Dr. Claudia Gunsch's lab must be acknowledged and thanked for sharing their space and wisdom, particularly (now) Dr. Thomas Worley-Morse, Carley Gwin, and Lauren Czaplicki, for their willingness to answer any and all microbiology questions from a civil engineer. Dr. Mark Wiesner must be similarly acknowledged for drilling mass balances into the brains of all his students (myself included).

Many thanks to Johnny Weddle at Comfort Engineers, Inc. in Durham, NC for doing what I could not.

Thanks to The Bill and Melinda Gates Foundation's Reinvent the Toilet Challenge for inspiring my advisor to design an innovative sanitation system.

Finally, of course, thank you to my family for endlessly supporting my pursuit of knowledge.

1. Introduction

1.1 Sanitation

Fecal sludge management is one of the most pressing environmental and public health issues facing the world today. It is estimated that some 2.5 billion people do not have access to adequate sanitation, which is costly and causes a number of complex health and societal problems (1). In developed nations, taxes and fees contribute to large scale treatment facilities which utilize settling, filtration, chemical, and biological treatment before the water is released back into the environment. Operation and maintenance costs alone (not including construction) for a wastewater treatment plant in the U.S. that processes 100,000 m^3 d^{-1} of wastewater are estimated to be about $340,000/month (2). This does not include administrative costs for environmental and health organizations which establish and enforce regulations for waste water treatment operations. The cost born by most US households is in the range of $20.00 to $90.00 per month, depending on factors like type of treatment required, water availability, and availability of subsidies. Though manageable for most people in the US, for many without economic opportunities the cost is not feasible.

The case in most less developed nations is entirely different. Generally, there is no infrastructure in rural areas through which to collect waste from homes and workplaces, let alone funds to allocate to construction, maintenance, access to and regulation of large-scale treatment facilities. As a result, open defecation is common.

When rudimentary sanitation exist, it is often simple pit latrines. If they are to be used continuously, pit latrines must be emptied, requiring pumps and transport equipment, which are often used to dispose of untreated waste directly into local water sources (3). Open defecation attracts flies and other pests, which transport germs and pathogens onto people and food. Physical safety is also a factor to consider in areas with poor sanitation, in that leaving the home to defecate can lead to assault, especially at night (1).

The economic and logistic issues preventing access to sanitation give rise to the real problem, which is diarrheal disease. Caused by bacterial, viral, and parasitic infections, diarrheal disease is directly correlated to poor hygiene and sanitation, and is often fatal or causes stunting in young children. The WHO estimates diarrheal diseases are the second leading cause of death in children under five years old, killing about 760,000 children every year (4).

Safe, effective, affordable, and widespread sanitation is an absolute necessity to address these grave statistics. As the problem of fecal waste management has become recognized, the global health and engineering communities have stepped forward with potential solutions, one type being onsite technologies. The benefits of these technologies are many, including that they do not require infrastructure for fecal waste transport and treatment in larger-scale treatment facilities, and generally use much less water and energy than sanitation relying on centralized facilities and sewer networks.

1.2 Overall System

This thesis is a contribution to development of an onsite sanitation technology, the purpose of which is to establish a low-cost, low-carbon footprint, self-sanitizing toilet. The treatment method is a combination of anaerobic digestions and heat sterilization, both of which are low-tech, inexpensive compared to many treatments, and potentially simpler to deploy and maintain.

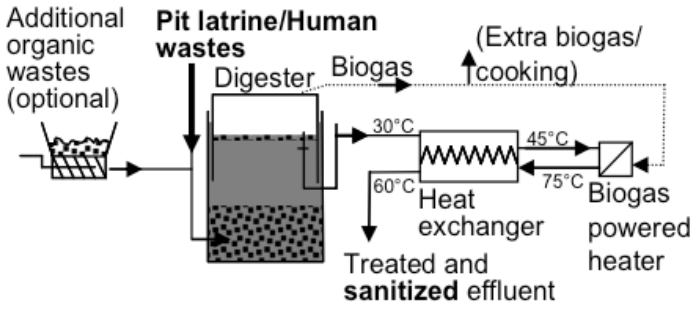

Figure 1: **Schematic of system (not to scale)**

Figure 1 is a conceptual schematic of the design, which consists of an anaerobic digester with two outputs - biogas and a treated waste slurry. The biogas powers a small heater while the slurry runs through a heat exchanger, into the heater, and back out through the exchanger. The temperature reached in the heater (>70 °C) serves to deactivate most microorganisms remaining in the treated waste effluent. The heat exchanger lowers the amount of biogas necessary to achieve the required temperature by using already heated slurry to increase the temperature of the slurry before it reaches the heater, serving as a safety factor and a cooler for the effluent (5). Because biogas is

provided by the waste itself, and all waste flows are driven by gravity, this fecal waste treatment system requires no energy input aside from the waste feed.

1.3 This Thesis: Modelling Heat Sterilization

In order to account for potential alterations in design, materials, sizing, and disinfection rates, and to accurately predict the system's ability to adequately sanitize waste, a model of the heat exchange and pathogen reduction was developed and validated. Assumptions were made about the available biogas (scaled based on measured values during laboratory experiments conducted by others) in order to create the model and test its value as a predicting tool for the larger system.

The present thesis is a comparison of the model's predictions to experimental data from a prototype. The main objective was to create a model that could closely predict the temperatures and pathogen concentrations throughout the system. The goals for achieving this objective were to:

- Develop a conceptual model based on heat transfer and pathogen decay kinetic equations
- Determine the appropriate parameters for the model as they related to heat, dispersion, and pathogen disinfection using experimentation when not provided in the literature
- Conduct experiments to verify the temperatures and pathogen concentrations simulated by the model
- Assess the accuracy of the model and provide recommendations for improvement and future research

The experimental methods, theory behind the development of the model, and a comparison of experimental results to model simulations are provided and discussed.

2. Model Development

2.1 Concept and Assumptions

A conceptual model was developed in Berkeley Madonna Software (version 8.3.18) in order to predict the system's ability to inactivate *E. coli*, viruses, and helminthes ova under varying conditions of flow, heater and exchanger material parameters, dimensions, and available power. Lab testing served to determine the model parameters, and the model was assessed with regard to temperature distribution and deactivation of pathogens within the system. Figure 2 shows a schematic representation of the heat exchanger and of the heater and transport processes in these devices. The color gradients seen in the arrows directing flow in the exchanger are a visual representation of the heat gained by the shell from the tube, and then lost from the shell. The black arrows depict the heat exchange across the steel tubing in the exchanger, and across the baffles within the heater, which has chambers numbered in flow order.

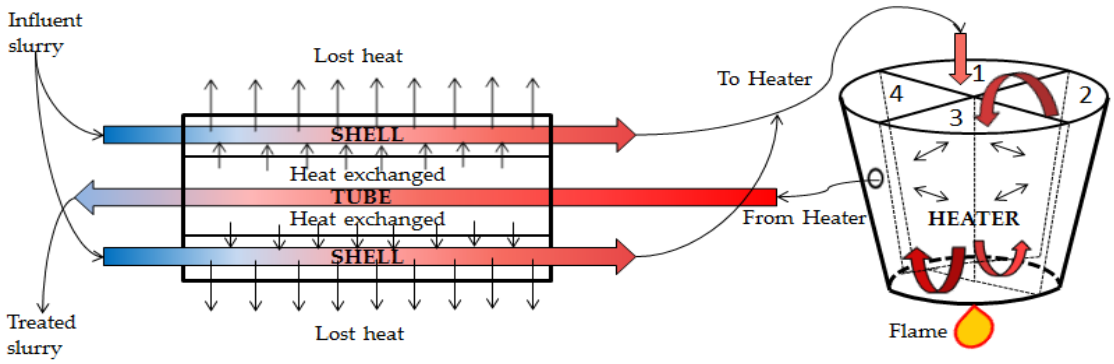

Figure 2: Schematic of flow in the system, direction of heat transfer indicated with arrows and color gradients (red=hot, blue=cold)

Assumptions were necessary to establish the differential equations used in the model.

1. The biogas and slurry flowrates from the digester are steady.
2. In order to represent the plug-flow nature of the heat exchanger it is modeled as a series of 20 completely mixed chambers, mimicking a plug flow reactor. The heater consists of 4 completely mixed identical chambers (corresponding to its actual construction).
3. Flow, conduction, convection, and dispersion of pathogens are the only phenomena considered (settling, sticking, growth, blockage, rust accumulation, etc. are neglected) for this initial analysis of the model, but others can be accounted for later.
4. The overall heat transfer coefficient, U, in the heat exchanger is a function of the liquid flowrate only, though the limitations of this will be discussed.
5. Other convective and conductive heat transfer coefficients are based on empirical equations and experimentation from the literature or described herein.
6. An Arrhenius equation is used to describe pathogen inactivation kinetics, which is widely used in microbiology, but sometimes oversimplifies the death kinetics.
7. No pathogen inactivation occurs at temperatures under 44℃.

In the following sections, model equations are developed. A symbol list defining the terms used in the model equations and specifying units used is available in Section 7.

2.2 Flow

Initially, the flowrate was based on the WHO estimates for volume of human waste produced per person per day and evenly distributed across 24 hours, such that 600 mL of water entered the system, over a period of five minutes, each hour. The tracer

tests were run using this flow pattern, but that was not feasible for the pathogen decay experiments, as feeding could not be automated. The pattern was therefore consolidated to 15 minute rather than one hour cycles (with 10 minute no-flow events), and the biogas flowrate was raised to allow the heater to reach the temperature it would during a one hour cycle. This pattern corresponded to the 15 minute cycle experiment discussed in subsequent sections.

In order to model the flow patterns used, periodic step functions established the discontinuous flow within the model. Using the commands seen in Lines 45-47 in Appendix A, a period of fifteen minutes with a five minute duration flow event allowed the model to experience the feed of 600 mL every fifteen minutes. The same commands were then used to establish the alternate peak flow pattern which is described as Lines 48-50 in Appendix A and correlates to the peak flows experiment discussed in subsequent sections.

2.3 Heat Transfer Equations

The distribution of temperature in the system was determined by using a series of differential equations, derived from a heat/energy balance on the discrete elements shown in Figure 4. Both heater and exchanger were modeled as having a series of completely mixed chambers. The number of chambers in each was set to 4 for the heater and 20 for the exchanger, represented by M and N in the equations, respectively. These numbers were chosen to mimic experimental data and to discretize the elements without

overwhelming the program with too many steps. Solving energy balances for $\frac{dT}{dt}$ gives the equations in Appendix A, which were required for Berkeley Madonna.

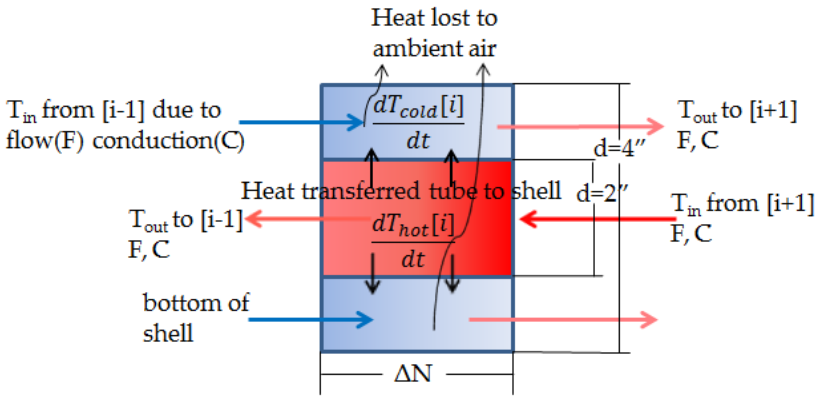

Figure 3: Cross sectional view of a chamber, i, in the heat exchanger, colored arrows represent the direction of flow and conduction, black arrows the heat exchange, thicker are between tube and shell, thinner are lost to atmosphere

While the equations for all the central chambers are similar, the first and Nth chambers each have terms for incoming and outgoing flow parameters and need to be written separately. Every equation has a term for flow in and out of the chamber, convective heat transfer between the hot and cold sections, conductive heat transfer between the chambers in series (i.e., in the axial direction), and loss to the atmosphere. FF is a cross sectional view of a single chamber indicating these phenomena with arrows. Equation 2, Equation 1, and Equation 3 are the heat balances (in Watts) for the shell sections of the heat exchanger. The left side of the equations represent the accumulation of thermal energy in a given exchanger chamber, i.e., the volume of water is equal to the total shell volume divided by N. The terms on the right are, sequentially, flow, heat transfer between tube and shell, axial conduction of water, and heat loss.

Solving for $\frac{dT}{dt}$ gives those equations in Appendix A which were required for Berkeley Madonna.

Shell First Chamber

$$V_{chamber} * \rho_{H2O} * Cp_{H2O} * \frac{dT_{shell}[1]}{dt} = Flow * \rho_{H2O} * Cp_{H2O} * (T_{shell}[in] - T_{shell}[i]) + U * SA_{tube} * (T_{tube}[i] - T_{shell}[i]) + k * A * \frac{(T_{shell}[i] - T_{shell}[i+1])}{\Delta N} - U_{loss} * SA_{shell} * (T_{shell}[i] - T_{amb})$$ Equation 1

Shell Middle Chambers

$$V_{chamber} * \rho_{H2O} * Cp_{H2O} * \frac{dT_{shell}[2 \dots N-1]}{dt} = Flow * \rho_{H2O} * Cp_{H2O} * (T_{shell}[i-1] - T_{shell}[i]) + U * SA_{tube} * (T_{tube}[i] - T_{shell}[i]) + k * A * \frac{(T_{shell}[i-1] - 2 * T_{shell}[i] + T_{shell}[i+1])}{\Delta N} - U_{loss} * SA_{shell} * (T_{shell}[i] - T_{amb})$$ Equation 2

Shell Last Chamber

$$V_{chamber} * \rho_{H2O} * Cp_{H2O} * \frac{dT_{shell}[N]}{dt} = Flow * \rho_{H2O} * Cp_{H2O} * (T_{shell}[i-1] - T_{shell}[i]) + U * SA_{tube} * (T_{tube}[i] - T_{shell}[i]) + k * A * \frac{(T_{shell}[i-1] - T_{shell}[i])}{\Delta N} - U_{loss} * SA_{shell} * (T_{shell}[i] - T_{amb})$$ Equation 3

The equations for the tube section are essentially the same as for the shell, with one difference, that is there is no term describing the losses to the ambient air. Also the input stream is different, since the inflow for the tube comes from the last chamber of the heater (see Equation 4).

Tube First Chamber

$$V_{chamber} * \rho_{H2O} * Cp_{H2O} * \frac{dT_{tube}[1]}{dt} = Flow * \rho_{H2O} * Cp_{H2O} * (T_{tube}[in] - T_{tube}[i]) - U * SA_{tube} * (T_{tube}[i] - T_{shell}[i]) - k * A * \frac{(T_{tube}[i] - T_{tube}[i+1])}{\Delta N} \quad \text{Equation 4}$$

The heat balance equations for the heater are as Equation 5, Equation **6**, and Equation **7**, with the terms defined in the Nomenclature.

Heater First Chamber

$$V_1 * \rho_{H2O} * Cp_{H2O} * \frac{dT_{heater}[1]}{dt} = F_{H2O} * (T_{cold}[N] - T_{heater}[i]) + Power * \propto + U_{heater} * SA_{baffle} * (T_{heater}[M] - 2 * T_{heater}[i] + T_{heater}[i+1]) \quad \text{Equation 5}$$

Heater Middle Chambers

$$V_{chamber} * \rho_{H2O} * Cp_{H2O} * \frac{dT_{heater}[2 \ldots M-1]}{dt} = F_{H2O} * (T_{heater}[i-1] - T_{heater}[i]) + Power * \propto + U_{heater} * SA_{baffle} * (T_{heater}[i-1] - 2 * T_{heater}[i] + T_{heater}[i+1]) \quad \text{Equation 6}$$

Heater Last Chamber

$$V_4 * \rho_{H2O} * Cp_{H2O} * \frac{dT_{heater}[M]}{dt} = F_{H2O} * (T_{heater}[i-1] - T_{heater}[i]) + Power * \propto + U_{heater} * SA_{baffle} * (T_{heater}[i-1] - 2 * T_{heater}[i] + T_{heater}[1]) \quad \text{Equation 7}$$

The accumulation of heat in a given heater chamber, as represented by the left side of the equations, is equal to the incoming heat subtracted by the outgoing heat. Therefore the first term of the right side of each equation is the heat carried into the chamber by the flow from the previous chamber subtracted by the heat carried into the next. The next is the heat delivered by the combustion of the biogas beneath the heater, followed by a term describing the heat exchange across the baffles of the heater. The subscripts define each parameter more specifically, and the symbol i refers to the chamber being analyzed.

2.4 Theoretical Overall Heat Transfer Coefficients

A tube-and-shell exchanger was chosen as the optimal design to minimize losses, since the hot tube would be insulated against atmospheric conditions by the shell (6). When sizing HE2, determining the optimal tube and shell diameters involved using the convection coefficients of the rectangular exchanger, HE1 and calculating the overall heat transfer coefficient using Equation 8 (5).

$$\frac{1}{U} = \frac{1}{h_{hot}} + \frac{1}{h_{cold}} + \frac{t}{K_{steel}} \qquad \text{Equation 8}$$

For a symmetrical rectangular heat exchanger with the same flow in both chambers like HE1, the convection coefficients of either section are equal, yielding Equation 9.

$$\frac{1}{U_{th}} = \frac{2}{h_{hot/cold}} + \frac{t}{K_s} \quad \text{Equation 9}$$

The average velocity in an exchanger is defined in Equation 10.

$$v_{avg} = \frac{F}{A} \quad \text{Equation 10}$$

The initial experiments during which the relationship between the overall heat transfer coefficient and the flowrate in HE1 was measured, provided Equation 11,

$$U_{th} = F * 7.996 + 15.85 \quad \text{Equation 11}$$

where the flow F is in L h^{-1}.

Plugging Equation 11 into Equation 9 and solving for h yields Equation 12,

$$h = \frac{2}{\left(\frac{1}{7.996(F)+15.85} - \frac{t}{K_s}\right)} \quad \text{Equation 12}$$

where Flow is given in Equation 13.

$$F = v_{hot\ or\ cold} * A_{box} \qquad \text{Equation 13}$$

Because the cross sectional areas of the hot and cold sections are not equal in a tube and shell exchanger, they have different fluid velocities for the same flow rate and thus different convection coefficients. Therefore the velocities, v_{hot} and v_{cold} were calculated using the cross sectional area of their respective sections. Using this relationship, a theoretical overall heat transfer coefficient, U_{th} for the tube and shell exchanger (HE2) was entered into the model to find and maximize the corresponding power exchanged in the heat exchanger for various size configurations.

Later, experimental determination of U was conducted. For this, hot water was circulated at a high flowrate on the tube side (or on the shell side) so that one could assume that the convection coefficient of the tube side was much larger compared to the other parameters in Equation 4, allowing this equation to be reduced to Equation 14.

$$\frac{1}{U_{conv}} = \frac{1}{h_{cold}} + \frac{t}{Ks} \qquad \text{Equation 14}$$

From there, h_{cold} could be determined using Equation 14 and Equation 21.

$$h_{cold} = \left(\frac{A * \Delta\text{Tlm}}{(Tout - Tin) * F * \rho * Cp} - \frac{t}{Ks}\right)^{-1} \qquad \text{Equation 15}$$

After inverting the experiment such that the shell was the hot section and the tube was the cold section, the convection coefficient h at each flowrate and for both sections could be determined. Then the overall heat transfer coefficient U_{conv} was calculated using Equation 21. It was compared to the results of U_{th} which were derived from HE1. Each of these was used in the model to identify the best fit to the experimental temperature data.

Heat losses from the heat exchangers needed to be included in the model. For this, the heat exchanger was filled with hot water and the temperature was allowed to equilibrate. Then the change in surface temperature of the heat exchanger over time was measured to determine U_{loss} i.e., the overall heat loss transfer coefficient. A curve fit of the shell temperature in the model to the measured temperature when the flow was set to zero was performed.

The overall heat transfer coefficient, U_{heater}, in the heater was determined by visually matching the model's predicted heater temperatures closely to the experimental temperature data during the pathogen decay experiments. Changing U_{heater} significantly altered the temperature difference between heater chambers, which was experimentally lower at high temperatures (15 minute cycle), and higher at low temperatures (peak flows). This was due to an increase in natural convection at higher temperatures, which increased the value of U_{heater}.

2.5 Biogas Production

Experiments conducted by others in our lab indicated that biogas production in the anaerobic digester provided roughly 10 L biogas for 0.3 persons per day. Scaling up, a value of 33.3 L biogas per person per day was chosen for the model. For scaling, the heating power provided to the heater is a function of the calorific value of methane, percent methane, biogas per person per day, and number of users, all of which can be adjusted for varying circumstances. This is shown in Equation 16.

$$Power = BG * capita * \%_{CH4} * cal_{CH4} * \rho_{CH4} * \propto \qquad \text{Equation 16}$$

2.6 Pathogen Removal

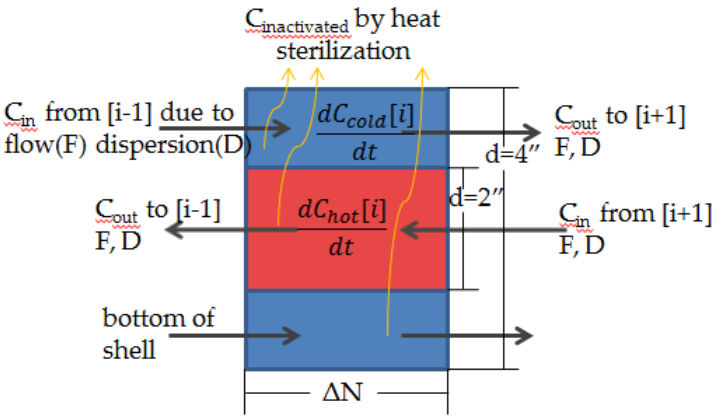

Figure 4: Cross sectional view of a chamber, i, in the heat exchanger, grey arrows represent the direction of flow, yellow arrows the heat inactivation of pathogens

The pathogen decay in the system is the ultimate objective of the heat sterilization system. Inactivation of pathogens was modeled according to the same method of completely mixed chambers (as for the temperature), but using a mass

balance rather than heat (5). Pathogen decay was directly dependent on the temperature in a given chamber (see Equation 17 and Figure 4). The inactivation coefficients were estimated by the Arrhenius equation which is given in Equation 17, in which the first order reaction rate coefficient was determined by temperature and the constants *Ea* and K_0.

Arrhenius

$$k = K_o * e^{\frac{-Ea}{R*T}} \qquad \text{Equation 17}$$

$$where\ \frac{d(C,V)}{dt} = -k * C * V$$

The constants, *Ea* and K_0 for each helminthe ova, viruses, and *E.coli* were found in the literature and are provided in Table 1 (9 and 5). Experiments were only conducted with *E. coli;* the intent was to calibrate and validate the model with *E. coli* and use the model to predict inactivation of other pathogens. In the model, a command was included such that k was equal to zero below 44 ^oC, i.e., no decay occurred below this threshold temperature. As listed in the assumptions, no growth of *E. coli* was included in the model. This is because experiments were conducted in water.

Table 1: **Pathogen Inactivation Constants**

	Ea (kJ/mol)	K_o (s^{-1})
E. coli	85.1	6.30E+13
Helminthe	105	4.04E+13
Viruses	39	2.00E+3

The mass balance equations were the same for the three pathogens examined by the model, only having different values of k, which varied with temperature. These were defined as kchamber_e, kchamber_h, or kchamber_v in the model code (where chamber is either the tube, shell, or heater chamber) for the coefficients of *E.coli*, helminthe ova, and viruses, respectively. Only those equations for *E.coli* are shown because the others are exactly the same but for the subscript on k.

The mass balance equations for *E. coli* in the shell are as in Equations 21-23 in which the left sides of the equations represent the change in cell concentration in a given chamber. The right sides of the equations represent sequentially, pathogens carried by the flow, heat inactivation, and dispersion. Solving for $\frac{dC}{dt}$ gives those equations in Appendix A which were required for Berkeley Madonna.

Shell First Chamber

$$V_{chamber} * d\frac{C_{cold_e[1]}}{dt} = Flow * \left(C_0 - C_{cold_e[i]}\right) - K_{cold_e[i]} * V_{H2O} * C_{cold_e[i]} - \frac{Dx}{\Delta N^2} * V_{chamber} * (C_{cold\_}e[i] - C_{cold\_}e[i+1])$$

Equation 18

Shell Middle Chambers

$$V_{chamber} * \frac{dC_{cold_e[2\ldots N-1]}}{dt} = Flow * \left(C_{cold_e[i-1]} - C_{cold_e[i]}\right) - K_{cold_e[i]} * V_{H2O} * C_{cold_e[i]} + \frac{Dx}{\Delta N^2} * V_{chamber} * (C_{cold\_}e[i-1] - 2 * C_{cold\_}e[i] + C_{cold\_}e[i+1])$$

Equation 19

Shell Last Chamber	$V_{chamber} * \frac{dC_{cold\_e[N]}}{dt} = Flow * (C_{cold\_e[i-1]} - C_{cold\_e[i]}) - K_{cold\_e[i]} * V_{H2O} * C_{cold\_e[i]} + \frac{Dx}{\Delta N^2} * V_{chamber} * (C_{cold\_e[i-1]} - C_{cold\_e[i]})$	Equation 20

The axial dispersion coefficients are represented by Dx and Dy for the exchanger and heater, respectively. Only the subscripts of the terms are different in the mass balances on the tube's chambers, while the $\frac{Dx}{\Delta N^2}$ term in the heater equations changes to $\frac{Dx}{\Delta M^2}$ where ΔM is the distance traveled through a heater chamber, i.e. the height.

The major limitation of the model was that the overall heat transfer coefficients must be determined experimentally if the other parameters such as sizing and materials change dramatically between designs. These experiments are described in the following chapter.

3. Materials and Methods

3.1 Heat Exchanger

The stainless steel 304 countercurrent tube and shell heat exchanger used in the most experiments (HE2) was constructed by Comfort Engineers, Inc. (Durham, NC) having 4.03 in. shell inner diameter, 2.07 in. tube inner diameter, wall thickness of 0.154 in, and insulated with silver foil bubble wrap. Earlier prototypes, built in-house, were used to construct the model and optimize sizing for the final products. The initial heat exchanger (HE1, see Figure 2) was constructed out of galvanized steel 0.285 in thick. It was a 28.0 in. long rectangular structure with two identical parallel chambers for the countercurrent hot and cold sections respectively, with one 3.74 in. tall wall for heat exchange. Each chamber of HE1 was 1.00 in. wide. The sizes of both heat exchangers were determined to be suitable for heat treatment of the waste generated by an extended family of 10, i.e., about 16-20 L per day, which correspond to the volume of fecal waste produced plus a minimal amount of flush water.

The overall heat transfer coefficient, U was first determined on HE1 (when equipped with fiberglass insulation) experimentally by measuring the temperature at the four critical points (all flow inlets and outlets) shown in Figure 5.

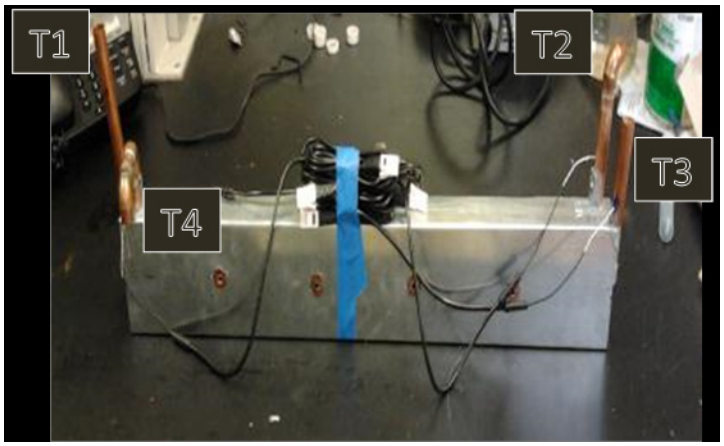

Figure 5: **Critical points of the heat exchanger: T1 = $T_{cold.in}$, T2 =$T_{cold.out}$, T3=$T_{hot.in}$, T4=$T_{hot.out}$**

Equation 21 was used to calculate the experimental overall heat transfer coefficient at flowrates of 2, 5, 10, and 20 L h^{-1} in HE1 (6). Tap water was pumped at a known flowrate, through points one and two, then to an electric water heater, and back through points three and four. Temperature sensors and data loggers (Vernier Software & Technology Beaverton, OR) were used to monitor the temperatures at the four critical points, which were recorded until steady state for each flowrate.

$$U_{exp} = \frac{(Tout - Tin) * F * \rho * Cp}{A * \Delta\mathrm{Tlm}} \qquad \text{Equation 21}$$

$$where\ \Delta\mathrm{Tlm} = \frac{(\Delta\mathrm{T1} - \Delta\mathrm{T2})}{\ln(\frac{\Delta\mathrm{T1}}{\Delta\mathrm{T2}})}$$

The overall heat transfer coefficient for HE2 was also determined using this method. A linear relationship between the overall heat transfer coefficients in HE2 and

the axial fluid velocity was found. These values were then compared to calculated U values which were derived from U obtained in the rectangular exchanger HE1.

A second method of determining the overall heat transfer coefficient relying on experimentally determined convective heat transfer coefficients on each side of the stainless steel wall was attempted in order to determine the best experimental method for finding U. This overall heat transfer coefficient was identified as U_{conv}. The method involved running hot water at 360 L h^{-1} through the tube, and room temperature water through the shell in the opposite direction at flowrates of 1.5, 5 then 10 L h^{-1}, in three separate runs. When the temperatures were approximately steady (55-60 ℃ in the tube, 30-35 ℃ in the shell) the temperatures at each of the four critical points were collected by Vernier temperature probes and data logger. This experiment was done again with the shell as the hot section and the tube as the cold, and the data used to determine convective heat transfer coefficients for each section as a function of flow.

The heat transfer coefficient for heat losses U_{loss} from the heat exchanger to its surrounding was determined as follows. First water at about 85 ℃ was pumped at a flowrate of 360 L h^{-1} through both tube and shell of HE2.When the temperature was approximately steady, the flow of hot water was discontinued. The decrease of temperature at the surface of the shell was measured by a Vernier (Beaverton, OR) temperature probe and data logger. U_{loss} was determined by fitting a model simulation

(see model description in Section 3.3) of HE2 (setting all flows to zero) to the experimental data.

3.2 Heater

The baffled heater was fabricated by Comfort Engineers, Inc. from stainless steel 304. Natural gas and a Bunsen burner were utilized for power. The bottom and top diameters of the heater were 10.00 in. and 12.00 in. respectively, was 14.00 in. tall, and had a wall thickness of 0.154 in.

The thermal efficiency of heater defined as thermal energy gained by the heated content divided by the heat of combustion of the burned gas was determined as follows. The heater was filled with water and heated with biogas and Bunsen burner up to about 80 °C while the biogas flowrate was measured with a Dwyer Instruments (Michigan City, IN) flowmeter. The temperature within the heater was measured with Vernier (Beaverton, OR) temperature sensors, and the efficiency at various heater temperatures calculated using Equation 22, where $\frac{dT}{dt}$ was the slope of the curve generated by the temperature increase over time.

$$\propto = \frac{\frac{dT}{dt} * \rho_{H2O} * V_{H2O} * Cp_{H2O}}{F_{gas} * \%CH4 * Cal_{CH4} * \rho_{CH4}} \qquad \text{Equation 22}$$

3.3 Tracer Tests

The tracer tests were conducted to determine the residence time, residence time distribution, and axial dispersion coefficient during both continuous flow and discontinuous flow. The latter operation represents best flow through the system during actual use (each time an individual uses the facility, a volume of effluent equal to the fecal waste produced is displaced). These experiments consisted of feeding a discontinuous flowrate of 600 mL of water over a period of five minutes (thereby simulating one use of the toilet), once each hour, with an initial pulse of 20 g NaCl included in 300 L of the first 600 L feed. These experiments were performed on the heater and heat exchanger separately to find their respective dispersion coefficients. Each piece of equipment was initially full of water, and the background and experimental conductivities (See section 4.4) were measured at the outlet point and collected by a Vernier conductivity probe and LabQuest data logger (Vernier Software & Technology Beaverton, OR). All dispersion coefficients and retention times were calculated using Equation 23 (5).

$$Var = 2\tau^2[\frac{D}{uL} - (\frac{D}{uL}^2)(1 - exp\left(-\frac{uL}{D}\right)] \quad \text{Equation 23}$$

In order to easily compare the heater retention times with and without baffles, a simple, continuous flow tracer test was conducted, using the same initial pulse of 20 g in 0.3 L but pumping a continuous flowrate of 12.5 L h^{-1} for both. All tracer tests were

conducted at room temperature, without heating (thus neglecting natural convective processes).

3.4 Pathogen Removal

An experiment was designed to assess the system's ability to inactivate pathogens and to verify the removal efficiencies generated by the mathematical model of the system. Two L of LB Broth were inoculated with *E. coli K-12* and incubated for 48 hours at 37 °C. The optical density (at 600 nm) of the broth after 48 h was about 0.89 which corresponded to approximately 6 x 10^8 CFU m L^{-1} on a standard growth curve (7). The broth was centrifuged, the cells resuspended in 1 L of phosphate buffer solution (per L: 8g NaCl, 0.2g KCl, 1.44g Na_2HPO_4, 0.24g KH_2PO_4), and diluted with DI water (40 mL solution into 1960 mL H_2O about 25 times) to achieve a feedstock of ~50L having a concentration of approximately 10^7 CFU/mL.

The system was fed 600 mL of the feedstock at 7.2 L-h^{-1} every fifteen minutes for 20 hours. Samples were taken after the 2, 3, 4, 10, 17, and 20 hour marks at each of the locations depicted in Figure 6 which includes the four critical points on the exchanger as well as the first three of the chambers in the heater (because the 4^{th} was the same temperature as point 6). Serial dilutions were performed on the first four sampling events in duplicate, and in triplicate on the last two. Samples were plated, and incubated for 20 hours at 37 °C to assess the colony count at each point over the course of the experiment. Because the system was fed every fifteen minutes rather than every hour (to

accelerate the experiment, but thereby increasing the heat demand), the biogas flow to the heater was set to 450 mL min^{-1} so it could reach the same temperature change in 10 minutes as in a 55 minute no-flow period. It was brought to temperature prior to experimentation to start near steady state.

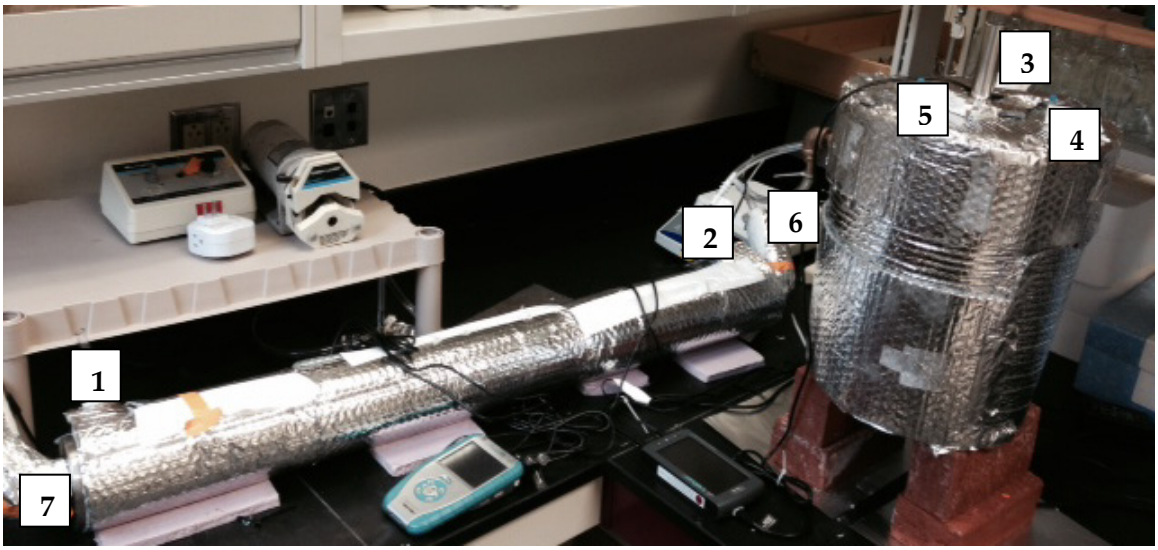

Figure 6: System setup indicating seven sampling points; 1: into shell, 2: leaving shell, 3-5: first three heater chambers, 6: leaving heater, 7: leaving shell

The parameters for deactivation of *E. coli* were adjusted in the model (see model and model parameter determination section for details), within the ranges found in the literature, such that the predicted log reductions at the critical points best matched those data from the 15 minute cycle experiment.

Verification of the model and effectiveness of the system was conducted in another experiment which analyzed the deactivation during more realistic flow conditions. These conditions were predicted based on water usage in El Pital, Honduras, a rural village in Central America, as observed by Engineers Without Borders- Santa

Clara University Student Chapter in 2011. Appendix B shows the predicted hourly distribution of waste into the digester, along with the adjusted simpler version used for experimentation.

Though the flow would not be continuous in the field, continuous flow was easier to automate in the lab, conservatively allowed fewer no-flow periods, during which the heater could come to a higher temperature. The 24-hour cycle depicted in Appendix B and described in

Table 2 was run for 68 hours, ensuring that the feed from one 24-hour cycle would have traveled all the way through the system. Samples were taken at hours 34, 44, 50, 54, 64, and 68 to correlate with the times the feeds would theoretically reach the selected sampling points, and diluted in duplicate for sampling points 1 and 2. Given anticipated reduction in *E. coli*, a standard membrane filtration method was used for sampling points 3-7; the volumes sampled were 1 mL and 10 mL.

Table 2: **24 hour cycle feeding schedule**

Hour	Flowrate (L h^{-1})
0-4	0
4-7	2.0
7-8	0
8-12	0.5
12-13	0
13-15	0.5
15-16	0
16-19	1.5
19-20	0
20-23	0.5
23-24	0

4. Results and Discussion

4.1 Optimal Sizing for HE2

Figure 7 shows the linear relationship that was obtained between the overall heat transfer coefficient of both sections, and the flowrate, determined experimentally and using Equation 21.

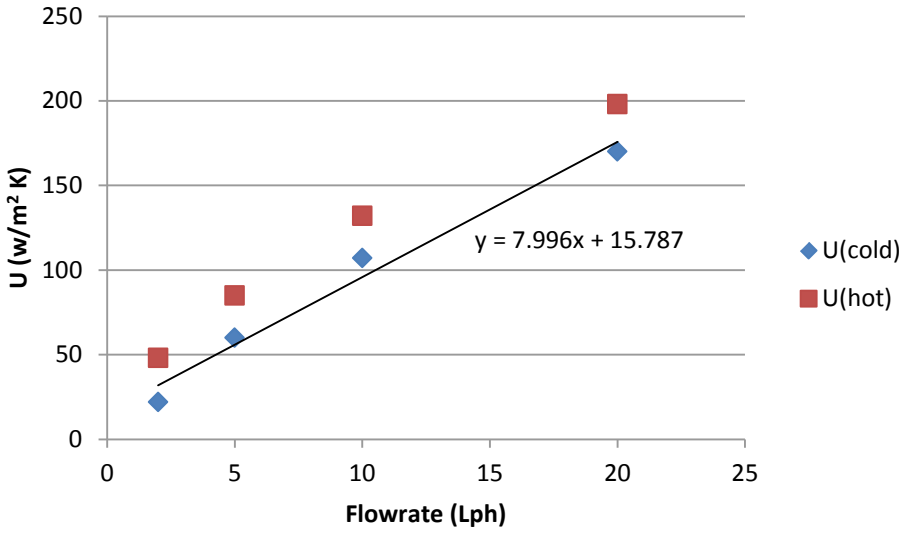

Figure 7: HE1 U_{cold} and U_{hot} refer to the fluid (cold or hot) being used to calculate $T_{out} - T_{in}$ (see Equation 1). Only the linear relationship of U based on the cold section is plotted.

The values for U are high due to the large surface area for heat exchange relative to the internal volume of either chamber in HE1. U_{hot} is higher than U_{cold} because the hot side transfers more heat than the cold side gains, due to losses. In an ideal exchanger without losses, all the heat transferred from the hot side would be gained by the cold side and the values would be equal.

The linear relationship between U_{cold} and flowrate was used for calculations described in Section 3.4 rather than the one based on $U_{hot,}$ to give a more conservative estimate for the rate of heat exchange. The equation displayed in the graph in Figure 4 was used to determine U_{th} which was then used in the model to find an optimal size for the tube and shell exchanger, HE2.

Table 3 shows various sizes that were entered in the model and using U_{th}, temperatures throughout the system were simulated. The table shows the corresponding calculation of power gained by the shell side liquid, determined by the model. The table shows a clear pattern; the larger the surface area for heat exchange and the smaller the shell diameter, the higher the power gained by the shell-side liquid in the exchanger. This was to be expected given the principles of heat exchange (6).

Table 3: **Calculated power gained in the shell at various tube and shell sizes, as predicted by the model**

Tube Diameter (inches)	Shell Diameter (inches)	Power Gained (Watts)
1	3	36.3
	4	32.4
	5	28.6
	6	24.8
1.5	3	41.1
	4	36.6
	5	32.2
	6	28.1
2	3	45.1
	4	39.9
	5	35.1
	6	30.6
2.5	3	49.0
	4	42.6
	5	37.4
	6	32.7
3	4	45.0
	5	39.4
	6	34.4

The 2″ and 4″ diameters for the hot and cold sections were chosen for their high predicted power, ease of construction in using common sizes, and in order to leave an inch, a standard plumbing minimum, for possible solids to pass through the exchanger. Increasing the heat exchanger length in the model showed an increase in power, which was to be expected given the greater surface area for heat exchange to occur, and a length of about one meter was chosen to keep the system at a functional size.

4.2 U_{exp} Determination

Once HE2 was fabricated, U_{exp} was characterized as a function of flowrate, as shown in Figure 8. A polynomial rather than a linear equation provided a more accurate fit of the data for U_{hot} which was used in this case rather than the more conservative U_{cold}, because the U_{loss} term would account for the difference between the hot and cold U values.

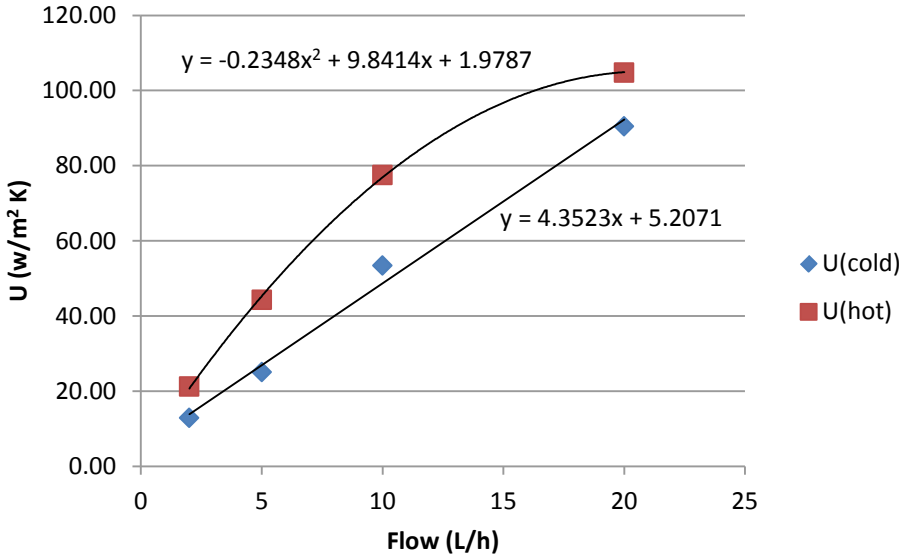

Figure 8: HE2 U(cold) and U(hot) [shell and tube] as a function of flowrate. Polynomial equation used as U_{exp}.

4.3 U_{loss} Determination

The change in the surface temperature of HE2 during U_{loss} determination experiments over time is shown in Figure 9. The model was then used to fit the shell temperature to these data to find U_{loss} which was 4.3 W/m²K. This value was lower than

expected, and only fit well with the first of the pathogen decay experiments, described in section 4.7.

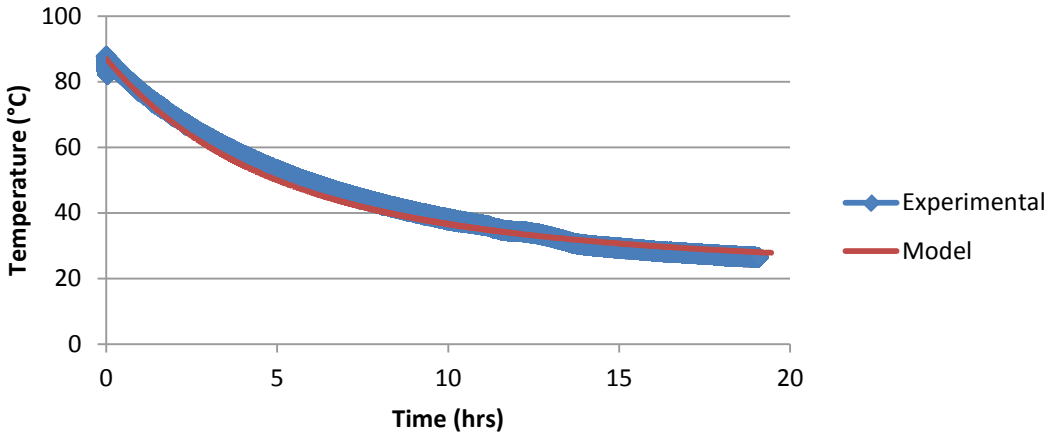

Figure 9: Surface temperature of the heat exchanger during no flow for the determination of U_{loss}. The red line is the model fitting while blue symbols are experimental data.

4.4 U_{conv} Determination

The linear relationships between the convection coefficients, h_{tube} and h_{shell}, and the flowrate of water through HE2 can be seen in Figure 10 below. These relationships were used in conjunction with Equation 11 (in section 3.4) to determine U_{conv} . It is interesting to note that below a flowrate of about 0.75 L h^{-1}, h_{shell} becomes negative, implying that the shell rapidly loses heat at low flow rates.

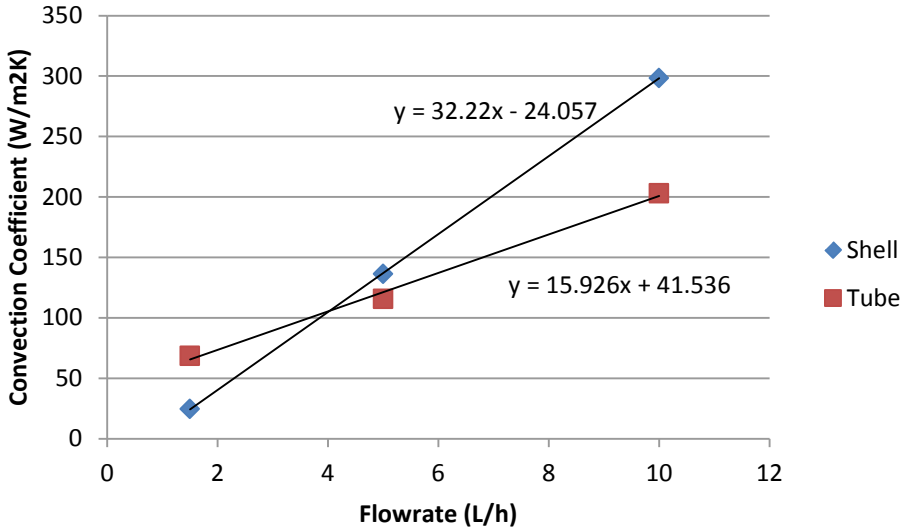

Figure 10: Convection coefficients in the heat exchanger, h_{tube} and h_{shell}, as a function of flowrate, obtained as described in sections 2.1 and 3.4 and used in Equation 11 to find U_{conv}.

4.5 Heater: U_{heater} and Thermal Efficiency

The values of U_{heater} for the two major pathogen removal experiments corresponding to biogas flowrates of 450 mL min^{-1} (15 min cycle) and 151 mL min^{-1} (Peak Flow) were 100 W/m^2K and 20 W/m^2K respectively for U_{heater} The increased natural convection present at the higher heating power accounts for the variation in U_{heater}.

The relationship between the thermal efficiency of the heater and the average temperature in the heater is shown in Figure 11. The efficiency, α, defined in Equation 22, was determined as 0.55 for the 15 minute cycle experiment and 0.70 for the peak flows experiment based on the experimental temperatures in the heater. The lower efficiency at higher temperature is caused by greater losses. Efficiency values could also

have been determined as a function of biogas flowrate rather than temperature to better understand the factors affecting efficiency. Even so, the relationship of α with temperature was sufficiently accurate to use for the model because these values are consistent with those in the literature.

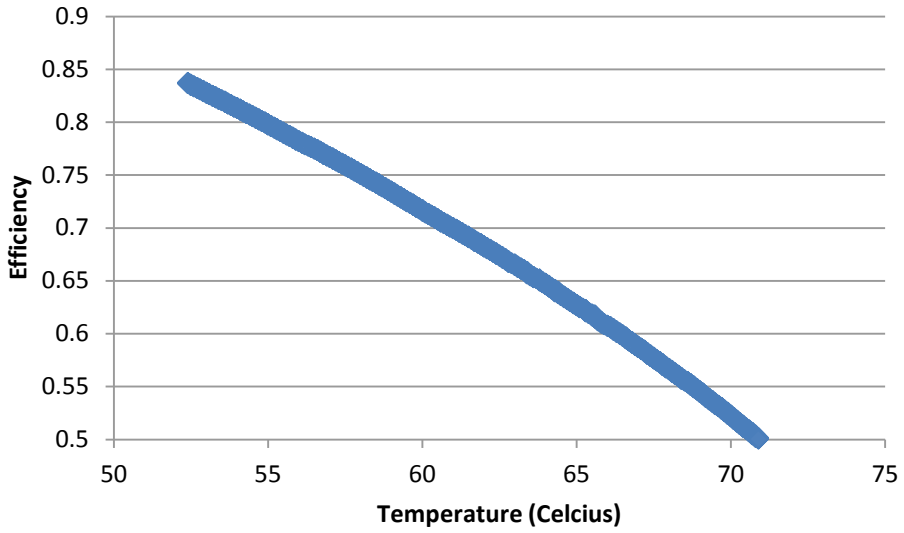

Figure 11: **Thermal efficiency of the heater as a function of its temperature**

4.6 Tracer Tests

The dispersion coefficients in **Table 4** correspond to the tracer tests done with one 600 mL feed for five minutes each hour. The raw data for these tests are in Appendix B. The experimental retention time for the entire system was 65.6 hours while the theoretical retention time was 49.6 hours. Of the 16 hour discrepancy, 15.5 are attributed to the heat exchanger, likely due to insufficient mixing of the tracer salt within the tube and shell, while the heater baffles provide natural mixing.

Table 4: **Dispersion coefficients (cm^2/s)**

	D (cm^2 s^{-1})
Heater	3.81E-08
Exchanger	2.86E-07

The retention times for the 12.5 L h^{-1} continuous flow tracer tests on the heater without and with baffles were 1.3 and 5.2 hours, respectively. The first is close to the theoretical retention time of 1.4 hours, but adding baffles quadrupled the retention time. It was expected that the heater without baffles would induce short circuiting and therefore reveal a lower retention time than the theoretical. It is clear that adding baffles allows more exposure time to higher temperatures.

4.7 Disinfection

4.7.1 U values

For the first disinfection experiment, the flowrate was either 7.2 L h^{-1} or 0 L h^{-1}, while flow for the peak flow experiment was varied bewteen 0, 0.5, 1.5, and 2 L h^{-1}. The values for U_{exp} and U_{conv}, corresponding to those flowrates and calculated from Figure 8, Figure 10, and Equation 8 are shown in **Table 5**. After several model simulations were conducted, it became clear that U_{exp} provided more accurate temperature estimates than U_{conv}. The remaining results only show those simulations which used U_{exp}.

Table 5: U_{exp} **and** U_{conv} **at experimental flowrates. Recall that** U_{exp} **is determined from Figure 8 while** U_{conv} **is determined from Figure 10 and Equation 8.**

Flowrate(L h^{-1})	Uexp (W/m^2-K)	Uconv (W/m2-K)
0.0	2.0	1.1
0.5	6.8	7.1
1.5	16.2	19.0
2.0	20.7	25.0
7.2	60.7	87.3

4.7.2 Fifteen Minute Cycle Experiment

Figure 12 shows the experimental temperature data for points 1 and 2 on either end of the shell, as well as the model simulated temperatures at those points, identified as Tcoldin and Tcoldout. The variation within a single cycle is a result of the increase in heat exchange during the five minute flow event and the heat conduction during the ten minute no-flow event. This variation is likely more extreme in the experimental data due to placement of the temperature sensor being close to the surface of the exchanger.

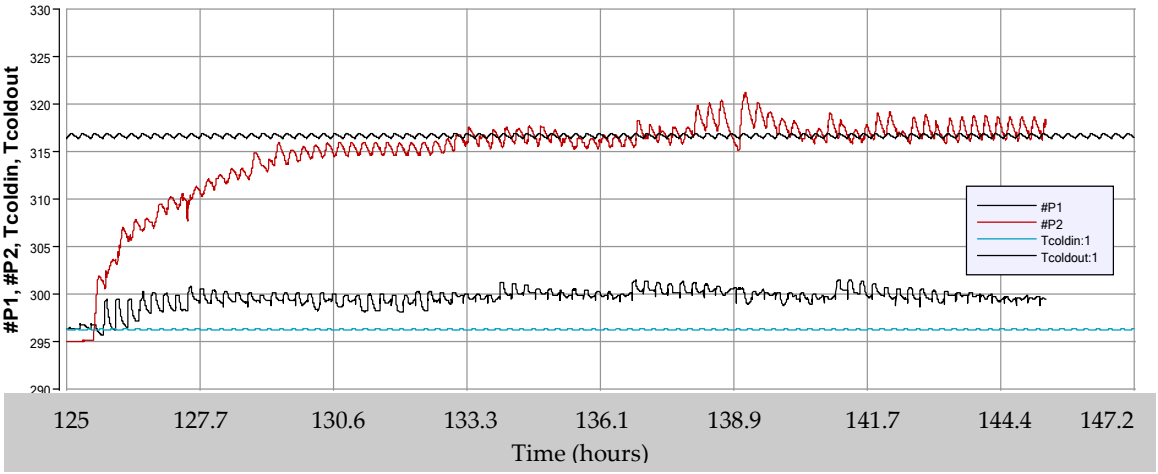

Figure 12: **Shell temperatures (in degrees K) during the 15 min cycle experiment, where P1 and P2 are the experimental data in the first and last chambers of the shell, and Tcoldin and Tcoldout are the model simulated temperatures at those chambers of the shell.**

The model predicts a heat gain in the shell of about 20 K while the experimental gain is only 16 K. The discrepancy is most likely due to slight error in the values for U_{exp} at no-flow (2.0 W m^{-2} K^{-1}) or U_{loss} (4.3 W m^{-2} K^{-1}). Tcoldin is estimated to be about 4 degrees too low, but it is more important that Tcoldout is a very close estimate because of the effects on pathogen disinfection closer to the heater.

Tcoldout serves as the starting temperature for the heater in the model, influencing subsequent temperature predictions. It is difficult to compare the model simulated heater temperatures to the experimental temperatures in

Figure 13 because only the first two chambers in the heater were measured (not enough sensors). The first chamber, H1, in the heater was hotter than the second, H2, which could have been due to the temperature probe in the first chamber being too close to the heater exhaust, too far in the second chamber, or possibly from inadequate insulation over the second chamber.

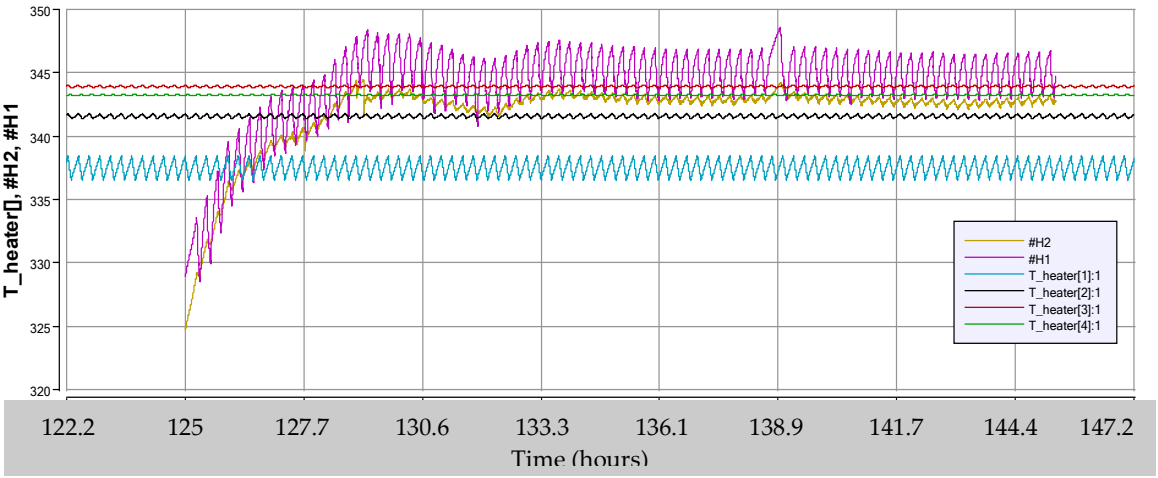

Figure 13: Heater temperatures (in °K) during the 15 min cycle experiment, where H1 and H2 are the experimental data in the first two heater chambers, and T_heater[1-4] are the model simulated temperatures in each of the 4 heater chambers.

The simulated temperature for the first chamber appears about 7 degrees low in Figure 13, which influences the second chamber which is predicted about 2 degrees low. Again, this is likely due to some error in the experimentation, as the first chamber in the heater should theoretically have the lowest temperature. The simulation also shows a higher temperature in the third chamber than in the fourth. This is possible as the liquid in the fourth chamber is losing heat to the first across the baffle before traveling into the tube of the heat exchanger.

Figure 14 depicts the experimental and simulated temperatures in the tube during the 15 minute cycle experiment. In the tube section of the heat exchanger, the experimental temperature for Thotin (the tube chamber closest to the heater, correlating

to P3 in the figure) is lower than expected. Some of the temperature probes could not physically reach all the way into the exchanger chambers, a weakness in the equipmental setup rather than the model, as P4 temperature is only slightly lower than the model simulated tube outlet.

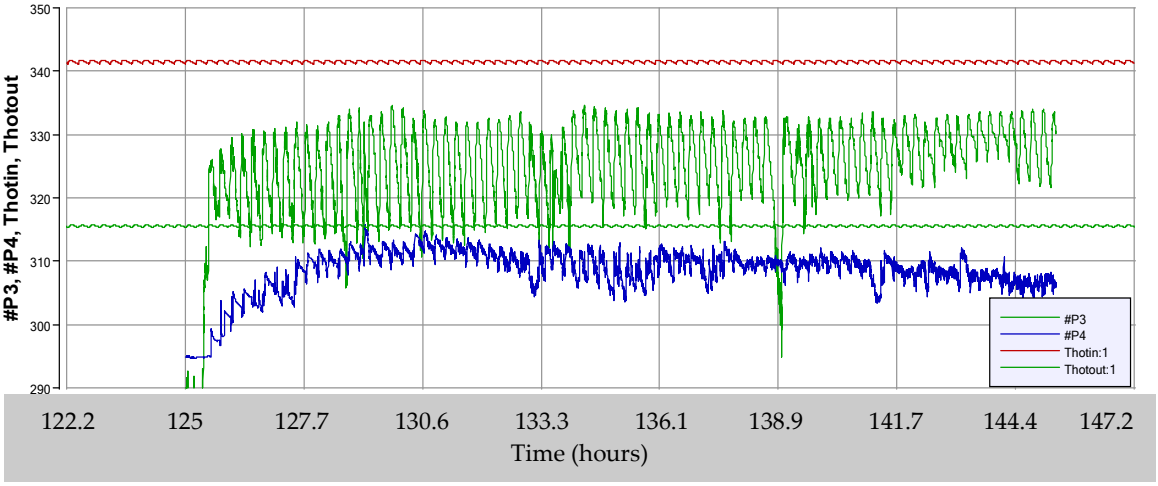

Figure 14: **Tube temperatures** (in °K) **during the 15 min cycle experiment, where P3 and P4 are the experimental data in the first and last chambers of the tube, and Thotin and Thot out are the model simulated temperatures at those chambers of the tube.**

The model does not account for losses in the tubing or variation in probe placement. As a result the simulated temperatures in the first entered chamber of the tube in Figure 14 are about 10 degrees higher than the experimental temperatures. This is less important for pathogen inhibition simulation than the temperatures in the shell and heater, because at this point the heater would likely have contributed the most to reducing pathogen concentrations, but it does represent a loss of thermal energy and effective insulation should be considered. However this could be mitigated by using longer temperature sensors that reach further into the exchanger. The wide variation in

the experimental temperature is an indication that the probe was not submerged or was not recording accurate data. Another explanation is that the pumps did not provide as consistent of flowrates as were expected.

E.coli was the only pathogen analyzed experimentally, so only those results are shown. The temperature simulations directly affect the pathogen concentration simulations, based on the Arrhenius equation. Figure 15 compares the experimentally determined *E. coli* concentrations to the model simulated values at the seven critical points identified in Figure 6. However, the comparison is somewhat moot, as the detection limits of the experiment, which were 3000 CFU mL^{-1} for points 1-4, and 300 CFU mL^{-1} for points 5-7, were too high and all analysis were below these levels. The model simulated concentrations of *E. coli* were essentially zero. Thus the model could not be adequately verified for this experiment.

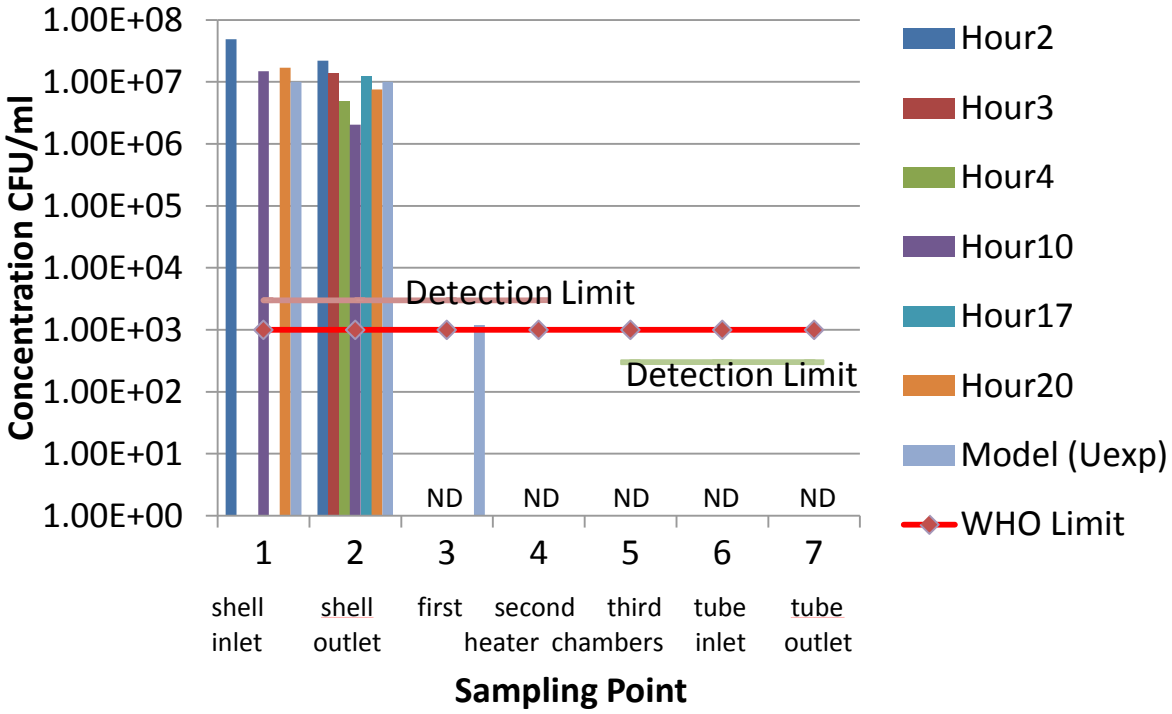

Figure 15: ***E. coli*** **concentrations at the sampling points and times during the fifteen minute cycle experiment, along with the model simulated concentrations at the sampling points.**

Too numerous of CFU counts from a previous experiment had led to the conclusion that these limits would be sufficiently low, but the higher temperatures had a larger effect on the CFU counts than was expected. Though the pathogen simulations in the model could not be verified for this experiment, it is promising to see that the deactivation was successful in this experiment. Repeating such experiments using membrane filtration to analyze *E coli* down to lower concentrations would be beneficial.

4.7.3 Peak Flows Experiment

Figure 16 shows the experimental temperature data for points 1 and 2 on either end of the shell as well as the model simulated temperatures at those points, identified as Tcoldin and Tcoldout. The far left peak in the graph is the temperature at the end of

the first flow event, and there should be five peaks in each 24 hour cycle to correspond to the five flow events shown in Table 2. The value for U_{loss} was left at 4.3 W $m^{-2}K^{-1}$, but comparing Tcoldout to Peak2 (model simulated v experimental shell outlet temperatures) in Figure 16 shows that this is either too low, or the value of U_{exp} is too high.

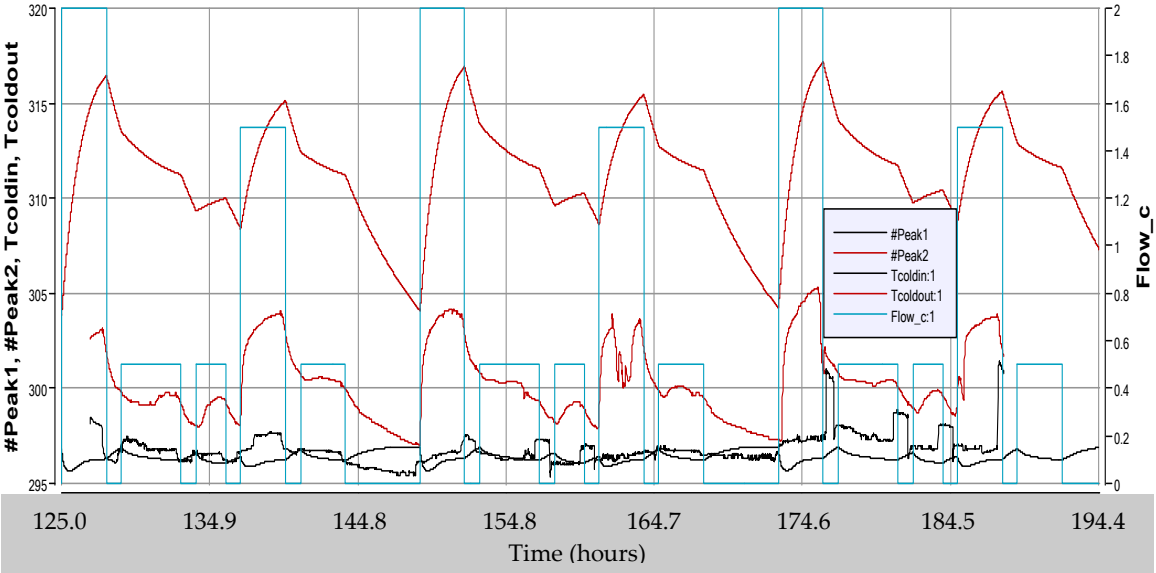

Figure 16: **Shell temperatures** (in °K) **during the peak flows experiment, where Flow_c is the flow pattern, Peak1 and Peak2 are the experimental data in the first and last chambers of the shell, and Tcoldin and Tcoldout are the model simulated temperatures at those chambers of the shell, using U_{loss}= 4.3 W $m^{-2}K^{-1}$.**

There is a plausible explanation for why there is such a discrepancy in the correct U values for the two experiments, which relates to the assumption that U is only influenced by the flowrate and not by temperature during no-flow events. In the ten minute no-flow event of the previous experiment, the tube and shell did not have time

to approach temperature equilibrium. During the one hour and five hour no-flow events of this experiment, as the two sections decrease in temperature, the overall heat transfer coefficient of loss, U_{loss} seems to increase significantly.

Because the U_{loss} determined by the curve fit did not match the experimental temperature data for the peak flows experiment, a larger value of U_{loss} = 20.0 W/m^{2}K was used. The results of a new simulation with this value are shown in Figure 17.

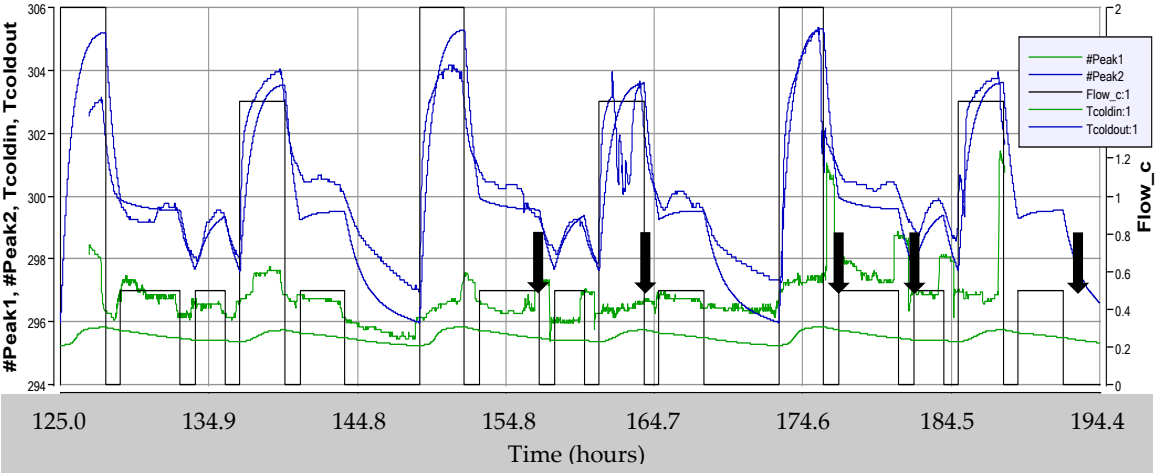

Figure 17: Shell temperatures (in °K) during the peak flows experiment, where Flow_c is the flow pattern, Peak1 and Peak2 are the experimental data in the first and last chambers of the shell, and Tcoldin and Tcoldout are the model simulated temperatures at those chambers of the shell, using U_{loss}= 20 W m^{-2}K^{-1}. The thick black arrows point out the sampling times.

It is clear that these data have closer matching trends, with peak flow events giving rise to higher temperatures and no-flow events causing the temperature to drop significantly. As in the 15 minute cycle experiment, Tcoldin is slightly underestimated.

Increasing the value of U_{loss} exaggerated the temperature decrease during no-flow events, but without that change, U_{exp} would be too high (even at the low value of 2 W $m^{-2}K^{-1}$. At very low flow rates, the standard relationship between U and flow is insufficient to describe the changing temperatures. It would be interesting to attempt to relate U_{exp} not only to the liquid flowrate, but to the biogas flowrate or the expected fluid temperature to account for the variation in natural convection within the exchanger during low or extremely low flow events.

The heater experimental temperature data for the peak flow experiment are noisier than the shell data. In **Figure 18**, PeakH1, PeakH2, and PeakH3 represent the experimental data. It can be seen by looking particularly at PeakH2 that the heater was gaining temperature over the course of the three day experiment. It may not have quite reached steady state but would approach the model simulated temperatures in **Figure 18** if the upward trend continued.

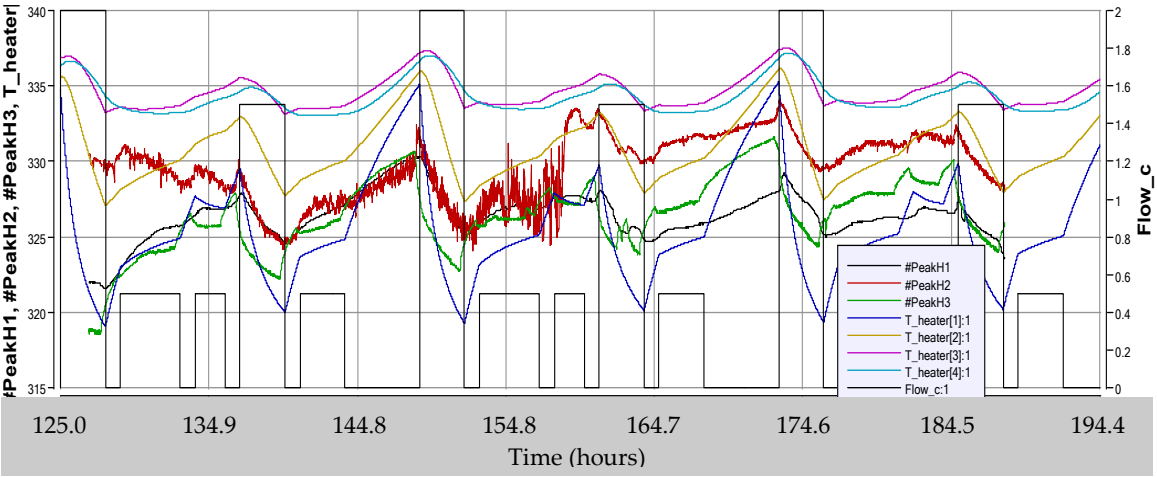

Figure 18: Heater temperatures (in °K) during the peak flows experiment, where Flow_c is the flow pattern, PeakH1, 2, and 3 are the experimental data in the first three heater chambers, and T_heater[1-4] are the simulated temperatures in the 4 heater chambers, using U_{loss}= 20.0 W $m^{-2}K^{-1}$

The model simulated heater temperatures for chambers 3 and 4 about 6 or 7 degrees higher than the sensor detected in chamber 3 (PeakH3), but Peak H3 seems to share trends with T_heater[1] and is cooler than was expected. The second chamber estimates are within 2 degrees during the last 24 hour cycle. The efficiency estimate of the heater may be set too high for these temperatures, but it is more likely that the heater in the experiment simply did not have time to reach steady state.

The temperature probes in the tube section malfunctioned during this experiment and are not shown. Neither is the model simulation as there is no way to make a proper comparison. **Figure 9** shows a comparison of the model simulated pathogen concentrations and the experimentally determined colony counts.

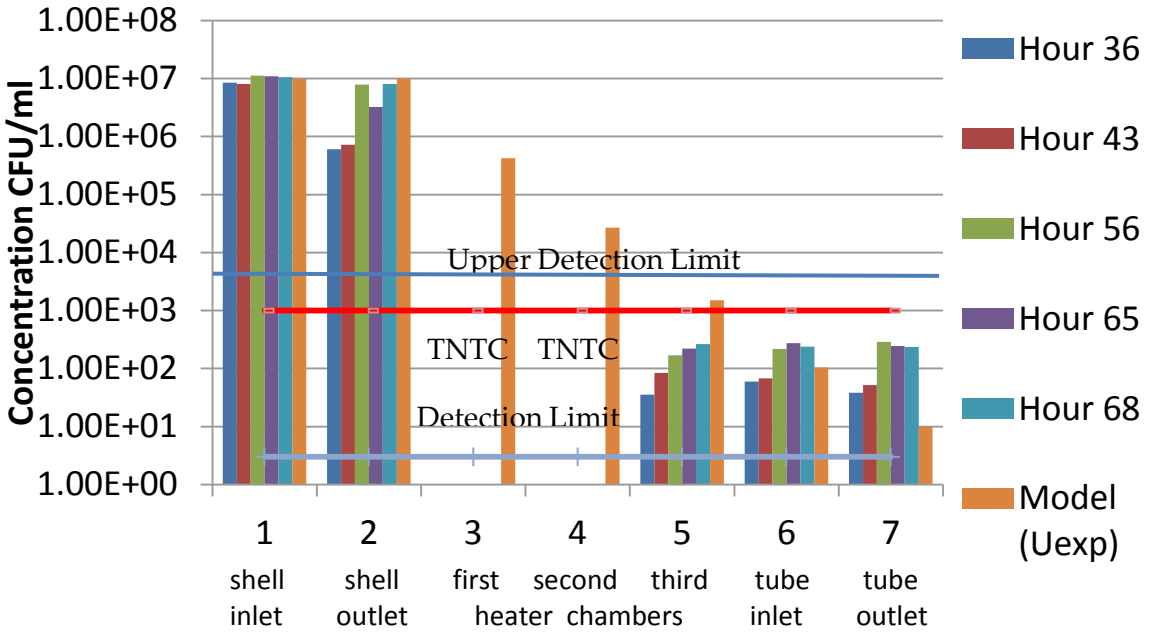

Figure 19: ***E. coli*** **concentrations at the sampling points and times during the peak flows experiment, along with the model simulated concentrations at the sampling points.**

The detection limit for points 3-7 of this experiment was 3.0 CFU/mL, which was low enough such that the model simulation could be more accurately verified than in the 15 minute cycle experiment. However **Figure 19** shows that the samples from points 3 and 4 were insufficiently diluted to determine their experimental concentrations. These could be attributed to inaccurate predictions due to the constants used in the Arrhenius equation for determining the reaction rate coefficient of *E. Coli*. The values were found in the literature but could be inaccurate, though this is difficult to determine given the limited data. They can easily be adjusted in the model to establish a more accurate fit of the pathogen concentration simulation or should be determined experimentally.

5. Recommendations for Future Research

5.1 Repeat/Improve Experiments

As discussed, validation of the model was only partial. Conducting new experiments for this project would be vastly improved simply by performing more comprehensive dilutions and membrane filtration volumes. Also, using additional temperature sensors at critical points would provide complete coverage of the system, and thus greater means of comparing the model predictions.

5.2 Uncertainties: Design New Experiments

Without improved data from those it is difficult to tell whether the pathogen decay constants were accurate, but specific experiment in flasks conducted at different temperatures to determine the values for K_0 and E_a would be relevant for this project as they would ensure accurate inactivation kinetic relationships as a function of temperature.

Validation of the heater model could also be improved by using more temperature sensors in each chamber, so that an average could be determined and offset the possible issues with temperature probe placement. It could serve to decide whether or not modeling the heater with 4 chambers is adequate.

The most uncertain parameter is the overall heat transfer coefficient at very low flow or no-flow events. Part of the issue is the difficulty of placing temperature sensors all the way into the chambers. If multiple sensors could be placed perpendicular to the

flow, in the first and last chambers in both tube and shell, a temperature gradient could be measured. Then, the U at no-flow could be more accurately determined as a function of temperature, by running water at the desired temperature through either section, and monitoring the temperature gradient and calculating the heat flux at selected temperatures.

5.3 Field Conditions

Another recommendation is closely analyzing the system in the field. As always in relocating from the lab to the field, unforeseen problems could arise. The conduction and convection coefficients will change as slurry is used and as slime develops on the inner surfaces of the equipment. The flow patterns will vary as will ambient temperature, wind, which will affect the losses.

5.4 Potential Additions

The Anaerobic Digester Pit Latrine (ADPL) system could be improved by utilizing passive solar energy to supplement heat to the system, which would reduce biogas consumption and making more of it available for other uses. Another addition which would improve the system would be better insulation than was used in these experiments. It would depend on the materials available in the field.

6. Conclusion

The experiments presented and discussed herein demonstrated that the heat exchanger/biogas-powered heater system as proposed could be a valuable device for sanitizing anaerobic digester effluents. Experiments conducted with *E.coli* achieved over four log reductions of cell counts over the system. This is a conservative estimate because of the way experiments were "accelerated" and actual cell residence time in the heat sterilization would be larger, with correspondingly greater cell deactivation. The heat exchanger did not contribute to a large viable cell reduction (one log reduction at the most) but was effective at recovering about 30% of total heat demand, thereby helping with the overall efficiency of the system. The model developed for this project estimates the temperatures across the heat exchanger and biogas powered heater fairly well considering the uncertainty of some parameters and the limited experimental data. The experimental temperature data was sufficient to show a decent fit of the model's predicted trends. The overall heat transfer coefficients could have been more accurately determined with further testing and with more precise and comprehensive experimentally determined temperatures. In the peak flows experiment, the model's pathogen concentration prediction for the first heater chamber was a bit higher than the experimental value in that chamber, and those in the final outlet of the system were a bit lower . Though widely used, the Arrhenius equation is not perfect for predicting microbial inactivation rates, and could be producing slightly skewed results. However

without more robust experimental data it is difficult to compare the pathogen concentrations.

If verified, the model could serve as a method of predicting the efficacy of this system in varying circumstances, where ADPL are deployed. The model should be a versatile tool. The available biogas production can be relatively easily predicted according to different feedstock and adjusted in the model. Similarly, the ambient temperatures can adjusted and varied over seasons, the scale of the pieces modified based on user size, and the reaction rate constants modified to simulate different pathogens. Since the model is based on concept and it captures fundamental phenomena occurring in the system, it should give reasonable estimates of the expected temperatures and pathogen disinfection. Overall, this project could serve as an important tool for sizing and assessing ADPLs and therefore help achieve safe onsite sanitation and contribute to the development of underprivileged communities.

7. Nomenclature

Some of the terms below have various subscripts which are used and defined throughout the text.

HE1	rectangular heat exchanger	ΔT1	=T4-T1
HE2	tube-and-shell heat exchanger	ΔT2	=T3-T2
T	temperature, K	A	area, m^2
F	flowrate, $m^3 s^{-1}$	D	dispersion coefficient, $cm^2 s^{-1}$
t	thickness, m	u	average velocity
K_s	heat transfer coefficient of steel, W $m^{-1} K^{-1}$	ρ	Density, kg m^{-3}
		V	Volume, m^3
U_{th}	theoretical overall heat transfer coefficient, derived from HE1 experimental data, W $m^{-2}K^{-1}$	Cp	Heat Capacity, J $kg^{-1} K^{-1}$
		L	Length, m
		Q	Heat, W
U_{exp}	experimental overall HT coeff., in relation to flowrate, W $m^{-2}K^{-1}$	Cal	Calorific Value of Methane, kJ kg^{-1}
		N	# of discrete chambers in HE2
U_{conv}	experimental overall HT coeff., in relation to convection coefficients, W $m^{-2}K^{-1}$	M	# of discrete chambers in Heater
		ΔN	Length of one discrete chamber in HE2=L/N, m
h_{tube}	convection coefficient of the tube, W $m^{-2}K^{-1}$	ΔM	Heater height, m
		SA	Surface Area, m^2
h_{shell}	convection coefficient of the shell, W $m^{-2}K^{-1}$	BG	biogas flowrate, $m^3 s^{-1}$
		$\%_{CH4}$	percent methane
ΔTlm	temperature log mean	τ	residence time, s
		α	efficiency

Appendix A Model Code

The following text is directly from the Berkeley Madonna Model Equations and was used for determining all the model predicted results. Anything within the '{}' symbols was supplemental text describing the equations and parameters and did not have any impact on the model output.

The periodic step function for the 15 minute cycle experiment and the IF THEN series describing the peak flows could not be used simultaneously. Therefore the periodic step functions for 15 minute as well as one hour cycles (which was used for preliminary model verification) are within '{}' symbols in this appendix.

There is also more than one equation for U, one being the experimental U and the other being the convection-related U. These can be differentiated by their supplemental descriptions, but only the polynomial relationship for U_{exp} is outside of brackets in this appendix. The placement of the brackets was simply changed for each various run of the model.

Some of the equations were used for reference points during verification and are not shown or discussed in the results section of the paper, but they have supplemental describing text in this appendix. Some parameters are listed in this appendix as having different values than those discussed in the results, such as Uloss and Uheat. These were easily adjusted in the parameter window of the model before each run according to the particular specifications of that run.

1. STARTTIME = 1
2. STOPTIME=7.5E+5
3. DT = 0.02

4. TIMEhours=TIME/3600

   {units in m, kg, s}

   {dimensions, m}

5. LL= 1.07 {length of heat exchange}
6. D1=.0547878 {Hot pipe inner D, m}
7. D2=.060325 {Hot pipe outer D, m}
8. D3=.1024 {Cold pipe inner D, m}
9. V_hot=((D1/2)^2)*PI*LL {Hot volume m3}
10. V_cold=((((D3/2)^2)-(D2/2)^2))*PI*LL {Cold volume m3}
11. Vn_hot = V_hot/N {vol one element}
12. Vn_cold = V_cold/N {vol one element}
13. deltaN = LL/N {length one discrete element, for conduction, m}
14. A_hotv=V_hot/LL {cross section area, for water conduction hot, m2}
15. A_coldv=V_cold/LL {cross section area, for water conduction cold, m2}
16. SA=D2*PI*LL {total surface area for exchange}
17. SAn=SA/n {area for heat exchange, one element}
18. xAheater=PI*(.125^2) {heater top area, m2}
19. SA_heat=.125*.30 {baffle area, m2}
20. H_heat=0.3 {heater height, m2}
21. N=20 {number of finite element for discretization-heat exchanger}

22. th=(D2-D1)/2 {thickness of steel, m}
23. Ks=20 {heat transfer stainless steel, W/mK}
24. k = 0.6 {water heat conductivity, W/m K}

25. Cp = 4180 {water heat capacity, J/kg K}
26. Ro = 1000 {water density, kg/m3}

27. HRTcold=(V_cold)/Fc {hydraulic retention time, shell, s}
28. vel_hot=Flow_c/A_hotv {surface velocity hot section, m/s}
29. vel_cold=Flow_c/A_coldv {surface velocity cold section, m/s}

30. h_hot=2/((1/(4.5107*A_hotv*vel_hot + 20.235))-(th/Ks)) {convection hot section,W/m2K}
31. h_cold=2/((1/(4.3523*A_coldv*vel_cold + 5.2071))-(th/Ks)) {convection hot section,W/m2K}

{
32. U =1/((1/h_hot)+(1/h_cold)+(th/Ks)) {Overall heat transfer coefficient, convection relationship, W/m2K}
}

33. U=-0.2348*(Flow_c^2) + 9.8414*Flow_c + 10 { Overall heat transfer coefficient, experimental polynomial relationship, W/m2K}

{
34. U=4.5107*Flow_c + 20.235 { Overall heat transfer coefficient, experimental linear relationship, hot, W/m2K }

35. U=4.3523*Flow_c + 5.2071 { Overall heat transfer coefficient, experimental linear relationship, cold, W/m2K }
}

36. Vcook =.018 {volume of heater, m3}
37. Vh_m = Vcook/M {vol of one CSTR in heater}
38. M=4 {number of chambers in heater}

39. Tcold_in = 300 {inlet temperature, K}

{makes input a periodic step function to model discontinuous flow}

{One hour cycle}
{
40. Flow_c = IF MOD(TIME+3300, period) >=thresh THEN cont_flow ELSE 0.00000001
41. period=3600
42. duration=300
43. thresh=period-duration
}

44. cont_flow=0.72*capita {estimated flow in L/h for five minutes each hour}

{15 minute cycle experiment}
{
45. Flow_c = IF MOD(TIME+600, period) >=thresh THEN cont_flow ELSE 0.00000001
46. period=900
47. duration=300
48. thresh=period-duration
}

{peak flows experiment}

49. Flow_c = IF((MOD(TIMEhours, period)>=5 AND MOD(TIMEhours, period)<8)) THEN 2 ELSE IF ((MOD(TIMEhours, period)>=9 AND MOD(TIMEhours, period)<13)) THEN 0.5 ELSE IF ((MOD(TIMEhours, period)>=14 AND MOD(TIMEhours, period)<16)) THEN 0.5 ELSE IF ((MOD(TIMEhours, period)>=17 AND MOD(TIMEhours, period)<20)) THEN 1.5 ELSE IF ((MOD(TIMEhours, period)>=21 AND MOD(TIMEhours, period)<24)) THEN 0.5 ELSE 0.00000000001

50. period=24

51. Flow_h = Flow_c {flow hot stream, equal to cold flow, L/h - }

52. d/dt (volcumul)=Fc {cumulative volume through system, m3}
53. INIT volcumul=0

{change unit}
54. Fc=Flow_c/(1000*3600) {m3/s}
55. Fh=Flow_h/(1000*3600) {m3/s}

{Info for curve fit and finding Uloss}

56. Aext=PI*D3*LL/N
57. Tamb=295
58. Uloss=4.29688 {lost heat transfer coefficient during no flow conditions}
59. Tshell=Tcold[1]

{Heat transfer in shell- change in temperature over time}

60. d/dt (Tcold[2..N-1]) = (Fc*Ro*Cp*(Tcold[i-1]-Tcold[i]) + U*SAn*(Thot[i]-Tcold[i]) + k*A_coldv*(Tcold[i-1]-2*Tcold[i]+Tcold[i+1])/deltaN - Uloss*Aext*(Tcold[i]-Tamb))/(Vn_cold*Ro*Cp)

{first element}

61. d/dt (Tcold[1]) = (Fc*Ro*Cp*(Tcold_in-Tcold[i]) + U*SAn*(Thot[i]-Tcold[i]) - k*A_coldv*(Tcold[i]-Tcold[i+1])/deltaN - Uloss*Aext*(Tcold[i]-Tamb))/(Vn_cold*Ro*Cp)

{last element}

62. d/dt (Tcold[N]) = (Fc*Ro*Cp*(Tcold[i-1]-Tcold[i]) + U*SAn*(Thot[i]-Tcold[i]) + k*A_coldv*(Tcold[i-1]-Tcold[i])/deltaN - Uloss*Aext*(Tcold[i]-Tamb))/(Vn_cold*Ro*Cp)

63. INIT Tcold[1..N]=300

{Heat transfer in tube- change in temperature over time}

64. d/dt (Thot[2..N-1]) = (Fc*Ro*Cp*(Thot[i+1]-Thot[i]) - U*SAn*(Thot[i]-Tcold[i]) + k*A_hotv*(Thot[i-1]-2*Thot[i]+Thot[i+1])/deltaN)/(Vn_hot*Ro*Cp)

{first element}

65. d/dt (Thot[1]) = (Fc*Ro*Cp*(Thot[i+1]-Thot[i]) - U*SAn*(Thot[i]-Tcold[i]) - k*A_hotv*(Thot[i]-Thot[i+1])/deltaN)/(Vn_hot*Ro*Cp)

{last element}

66. d/dt (Thot[N]) = (Fc*Ro*Cp*(T_heater[m]-Thot[i]) - U*SAn*(Thot[i]-Tcold[i]) + k*A_hotv*(Thot[i-1]-Thot[i])/deltaN)/(Vn_hot*Ro*Cp)

67. INIT Thot[1..N]=T_heater[M]

{Overall change in temperature, shell and tube}

68. deltaTinout_cold=Tcold[N]-Tcold_in
69. deltaTinout_hot=T_heater[m]-Thot[1]

{Power gained by heat exchange}

70. PWR_exch=Fc*ro*Cp*deltaTinout_cold

{Heater Overall Heat Transfer Coefficient}
71. Uheat=20

{temperature in heater}

72. d/dt (T_heater[1]) = (Fc/Vh_m)*(Tcold[N]-T_heater[i]) + ((Power*Alpha/m)
+(Uheat)*SA_heat*(T_heater[m]-2*T_heater[i]+T_heater[i+1]))/(Vh_m*Ro*Cp)

73. d/dt (T_heater[2..m-1]) = (Fc/Vh_m)*(T_heater[i-1]-T_heater[i]) +
((Power*Alpha/m)
+(Uheat)*SA_heat*(T_heater[i-1]-2*T_heater[i]+T_heater[i+1]))/(Vh_m*Ro*Cp)

74. d/dt (T_heater[m]) = (Fc/Vh_m)*(T_heater[i-1]-T_heater[i]) +
((Power*Alpha/m)
+(Uheat)*SA_heat*(T_heater[i-1]-2*T_heater[i]+T_heater[1]))/(Vh_m*Ro*Cp)

75. INIT T_heater[1..m] = Tcold[N]

{Power as function of biogas/capita}
{
76. BG=7.5E-7 {biogas flow for 15 minute cycle, m3/ s}
}
77. BG=.0333 /(24*3600) {biogas flow per capita ,m3/person/s}

78. capita=10 {number of people}
79. CH4=.65 {methane content of biogas}
80. cal=50000000 {calorific value of methane, J/kg}
81. RoCH4=0.66 {density of methane, kg/m3}

82. Power= BG*capita*CH4*cal*RoCH4*Alpha

83. efficiency=0.7
84. Alpha = efficiency

{Pathogen Disinfection Rates}
85. R = 8.3145 {ideal gas constant, J/molK}
86. Co = 1e7 {CFU/mL}
87. Dx=1e-9 { axial dispersion in exchanger m2/s}
88. Dy=1e-9 {dispersion in heater m2/s}

89. deltaM=0.2 {travel distance through heater chamber, m}

{for E. coli}

90. Ea_e= 85090 {J/mol}
91. Ko_e= 6.3e13 {/s}

92. Kcold_e[1..N] = IF (Tcold[i] >=317) THEN Ko_e*EXP(-Ea_e/(R*Tcold[i])) ELSE 0

93. Khot_e[1..N] =Ko_e*EXP(-Ea_e/(R*Thot[i]))

94. Kheater_e[1..M] = Ko_e*EXP(-Ea_e/(R*T_heater[i]))

{E. coli removal in cold section}

95. INIT Ccold_e[1..N] = Co

96. d/dt (Ccold_e[1]) = (Fc/Vn_cold)* (Co - Ccold_e[i]) - (Kcold_e[i]*Ccold_e[i]) -((Dx/(deltaN^2))*(Ccold_e[i]-Ccold_e[i+1]))

97. d/dt (Ccold_e[2..N-1]) = (Fc/Vn_cold)* (Ccold_e[i-1] - Ccold_e[i]) - (Kcold_e[i]*Ccold_e[i])
+((Dx/(deltaN^2))*(Ccold_e[i-1]-2*Ccold_e[i]+Ccold_e[i+1]))

98. d/dt (Ccold_e[N]) = (Fc/Vn_cold)* (Ccold_e[i-1] - Ccold_e[i]) - (Kcold_e[i]*Ccold_e[i])
+((Dx/(deltaN^2))*(Ccold_e[i-1]-Ccold_e[i]))

{E. coli removal in heater}

99. INIT C_heater_e[1..M] = Ccold_e[N]

100. d/dt (C_heater_e[1]) = (Fc/Vh_m)* (Ccold_e[N] - C_heater_e[i]) - Kheater_e[i]*C_heater_e[i]-((Dy/(deltaM^2))*(Ccold_e[i]-Ccold_e[i+1]))

101. d/dt (C_heater_e[2..M-1]) = (Fc/Vh_m)* (C_heater_e[i-1] - C_heater_e[i]) - Kheater_e[i]*C_heater_e[i]+((Dy/(deltaM^2))*(Ccold_e[i-1]-2*Ccold_e[i]+Ccold_e[i+1]))

```
d/dt (C_heater_e[M]) = ( Fc/Vh_m )* (C_heater_e[i-1] - C_heater_e[i]) -
Kheater_e[i]*C_heater_e[i]+((Dy/(deltaM^2))*(Ccold_e[i-1]-Ccold_e[i]))

        {E. coli removal in hot section}
INIT Chot_e[1..N] = C_heater_e[M]

d/dt (Chot_e[N]) = ( Fc/Vn_hot )* (C_heater_e[m] - Chot_e[i]) -
Khot_e[i]*Chot_e[i]
-((Dx/(deltaN^2))*(Ccold_e[i]-Ccold_e[i-1]))

d/dt (Chot_e[2..N-1]) = ( Fc/Vn_hot )* (Chot_e[i+1] - Chot_e[i]) -
Khot_e[i]*Chot_e[i]
+((Dx/(deltaN^2))*(Ccold_e[i+1]-2*Ccold_e[i]+Ccold_e[i-1]))

d/dt (Chot_e[1]) = ( Fc/Vn_hot )* (Chot_e[i+1] - Chot_e[i]) - Khot_e[i]*Chot_e[i]
+((Dx/(deltaN^2))*(Ccold_e[i+1]-Ccold_e[i]))

limit Ccold_e>=1
limit Chot_e>=1
limit C_heater_e>=1

log_reductions_e=log10(Co)-log10(Chot_e[1])


        {for helminthes}
Ea_h=105000 {mol/J}
Ko_h= 4.03706*10^13 {/s}

Kcold_h[1..N] =  IF (Tcold[i] >=317) THEN Ko_h*EXP(-Ea_h/(R*Tcold[i]))  ELSE 0
Khot_h[1..N] = Ko_h*EXP(-Ea_h/(R*Thot[i]))
Kheater_h[1..M] = Ko_h*EXP(-Ea_h/(R*T_heater[i]))

        {Helminthe removal in cold section}
INIT Ccold_h[1..N] = co

d/dt (Ccold_h[1]) = ( Fc/Vn_cold )* (Co - Ccold_h[i]) - Kcold_h[i]*Ccold_h[i]
-((Dx/(deltaN^2))*(Ccold_h[i]-Ccold_h[i+1]))
```

```
118.  d/dt (Ccold_h[2..N-1]) = ( Fc/Vn_cold )* (Ccold_h[i-1] - Ccold_h[i]) -
      Kcold_h[i]*Ccold_h[i]+((Dx/(deltaN^2))*(Ccold_h[i-1]-2*Ccold_h[i]+Ccold_h[i+1]))

119.  d/dt (Ccold_h[N]) = ( Fc/Vn_cold )* (Ccold_h[i-1] - Ccold_h[i]) -
      Kcold_h[i]*Ccold_h[i]
      +((Dx/(deltaN^2))*(Ccold_h[i-1]-Ccold_h[i]))


            {Helminthe removal in heater}
120.  INIT C_heater_h[1..M] = Ccold_h[N]

121.  d/dt (C_heater_h[1]) = ( Fc/Vh_m )* (Ccold_h[N] - C_heater_h[i]) -
      Kheater_h[i]*C_heater_h[i]-((Dy/(deltaM^2))*(C_heater_h[i]-C_heater_h[i+1]))

122.  d/dt (C_heater_h[2..M-1]) = ( Fc/Vh_m )* (C_heater_h[i-1] - C_heater_h[i]) -
      Kheater_h[i]*C_heater_h[i]+((Dy/(deltaM^2))*(C_heater_h[i-1]-
      2*C_heater_h[i]+C_heater_h[i+1]))

123.  d/dt (C_heater_h[M]) = ( Fc/Vh_m )* (C_heater_h[i-1] - C_heater_h[i]) -
      Kheater_h[i]*C_heater_h[i]+((Dy/(deltaM^2))*(C_heater_h[i-1]-C_heater_h[i]))


            {Helminthe removal in hot section}
124.  INIT Chot_h[1..N] = C_heater_h[M]

125.  d/dt (Chot_h[N]) = ( Fc/Vn_hot )* (C_heater_h[m] - Chot_h[i]) -
      Khot_h[i]*Chot_h[i]
      -((Dx/(deltaN^2))*(Chot_h[i]-Chot_h[i-1]))

126.  d/dt (Chot_h[2..N-1]) = ( Fc/Vn_hot )* (Chot_h[i+1] - Chot_h[i]) -
      Khot_h[i]*Chot_h[i]
      +((Dx/(deltaN^2))*(Chot_h[i+1]-2*Chot_h[i]+Chot_h[i-1]))

127.  d/dt (Chot_h[1]) = ( Fc/Vn_hot )* (Chot_h[i+1] - Chot_h[i]) - Khot_h[i]*Chot_h[i]
      +((Dx/(deltaN^2))*(Chot_h[i+1]-Chot_h[i]))


128.  limit Ccold_h>=1
129.  limit Chot_h>=1
```

130. limit C_heater_h>=1

131. log_reductions_h=log10(Co)-log10(Chot_h[1])

{for viruses}

132. Ea_v=39000 {mol/J}
133. Ko_v = 1998.976 {/s}

134. Kcold_v[1..N] = IF (Tcold[i] >=317) THEN Ko_v*EXP(-Ea_v/(R*Tcold[i])) ELSE 0
135. Khot_v[1..N] = Ko_v*EXP(-Ea_v/(R*Thot[i]))
136. Kheater_v[1..M] = Ko_v*EXP(-Ea_v/(R*T_heater[i]))

{Virus removal in cold section}

137. INIT Ccold_v[1..N] = co

138. d/dt (Ccold_v[1]) = (Fc/Vn_cold)* (Co - Ccold_v[i]) - Kcold_v[i]*Ccold_v[i]
-((Dx/(deltaN^2))*(Ccold_v[i]-Ccold_v[i+1]))

139. d/dt (Ccold_v[2..N-1]) = (Fc/Vn_cold)* (Ccold_v[i-1] - Ccold_v[i]) -
Kcold_v[i]*Ccold_v[i]
+((Dx/(deltaN^2))*(Ccold_v[i-1]-2*Ccold_v[i]+Ccold_v[i+1]))

140. d/dt (Ccold_v[N]) = (Fc/Vn_cold)* (Ccold_v[i-1] - Ccold_v[i]) -
Kcold_v[i]*Ccold_v[i]
+((Dx/(deltaN^2))*(Ccold_v[i-1]-Ccold_v[i]))

{Virus removal in heater}

141. INIT C_heater_v[1..M] = Ccold_v[N]

142. d/dt (C_heater_v[1]) = (Fc/Vh_m)* (Ccold_v[N] - C_heater_v[i]) -
Kheater_v[i]*C_heater_v[i]-((Dy/(deltaM^2))*(C_heater_v[i]-C_heater_v[i+1]))

143. d/dt (C_heater_v[2..M-1]) = (Fc/Vh_m)* (C_heater_v[i-1] - C_heater_v[i]) -
Kheater_v[i]*C_heater_v[i]+((Dy/(deltaM^2))*(C_heater_v[i-1]-
2*C_heater_v[i]+C_heater_v[i+1]))

144. d/dt (C_heater_v[M]) = (Fc/Vh_m)* (C_heater_v[i-1] - C_heater_v[i]) - Kheater_v[i]*C_heater_v[i]+((Dy/(deltaM^2))*(C_heater_v[i-1]-C_heater_v[i]))

{Virus removal in hot section}

145. INIT Chot_v[1..N] = C_heater_v[M]

146. d/dt (Chot_v[N]) = (Fc/Vn_hot)* (C_heater_v[m] - Chot_v[i]) - Khot_v[i]*Chot_v[i]
-((Dx/(deltaN^2))*(Chot_v[i]-Chot_v[i-1]))

147. d/dt (Chot_v[2..N-1]) = (Fc/Vn_hot)* (Chot_v[i+1] - Chot_v[i]) - Khot_v[i]*Chot_v[i]
+((Dx/(deltaN^2))*(Chot_v[i+1]-2*Chot_v[i]+Chot_v[i-1]))

148. d/dt (Chot_v[1]) = (Fc/Vn_hot)* (Chot_v[i+1] - Chot_v[i]) - Khot_v[i]*Chot_v[i]
+((Dx/(deltaN^2))*(Chot_v[i+1]-Chot_v[i]))

149. limit Ccold_v>=1
150. limit Chot_v>=1
151. limit C_heater_v>=1

152. log_reductions_v=log10(Co)-log10(Chot_v[1])

Appendix B Supplemental Data

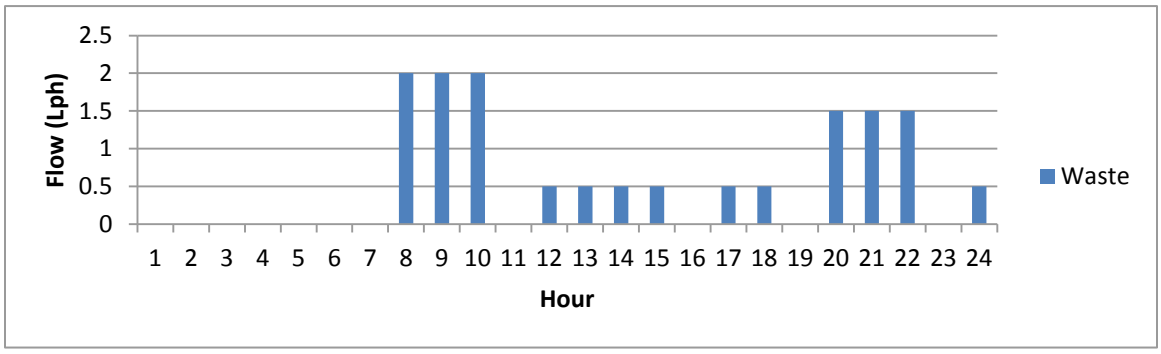

Predicted waste flowrates over a 24 hour cycle based on data from Engineers Without Borders- Santa Clara University Student Chapter

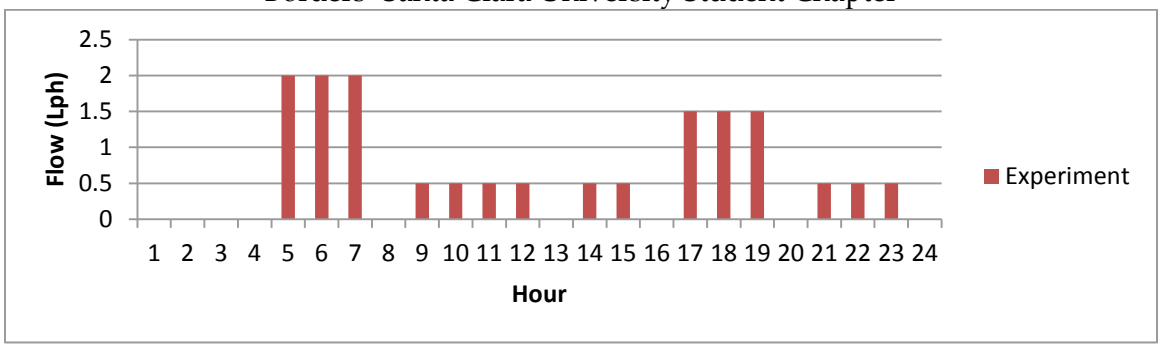

Simplified waste flowrate for experimentation during the peak flows experiment

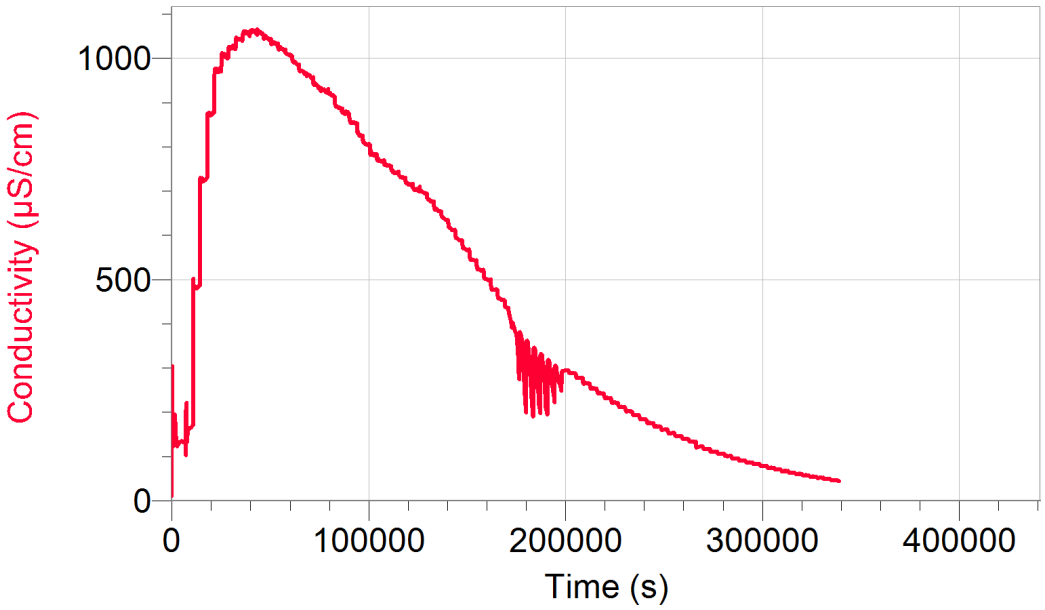

Data from tracer test on Heater

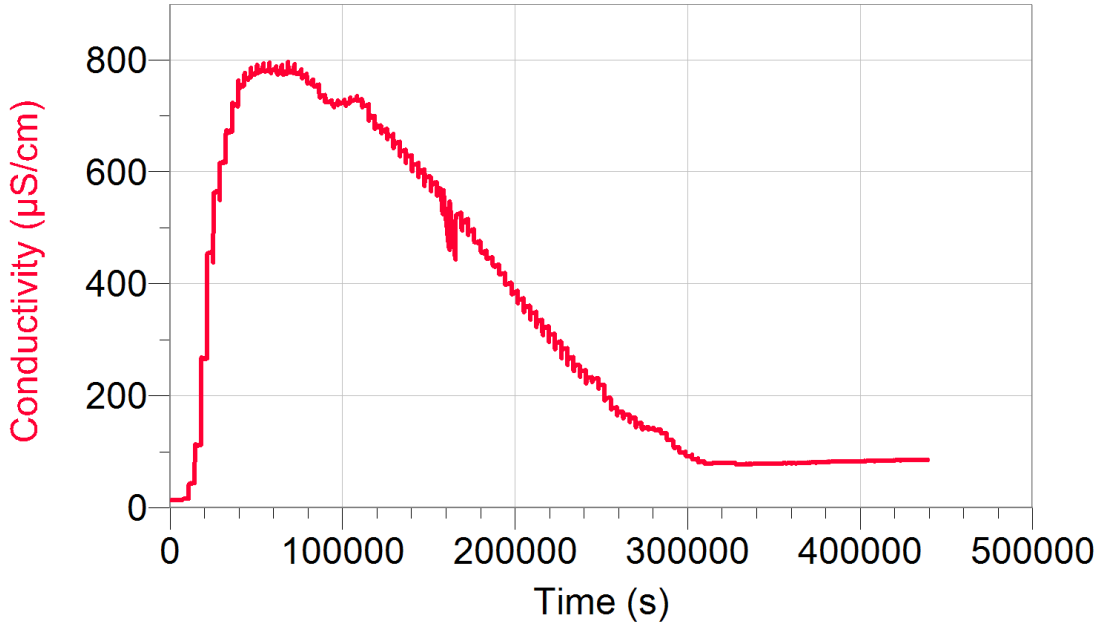

Data from tracer test on Exchanger

References

1. *Urgent Call to Action on Sanitation,* World Health Organization (WHO), 2013. Web 13 June 2014. http://www.who.int/water_sanitation_health/sanitation/action/en/

2. *Wastewater Treatment Plant Running* (2013) Cost Web 13 June 2014. http://www.costwater.com/runningcostwastewater.htm

3. Strand, Linda. "Faecal Waste: the next sanitation challenge." *Water 21.* June 2014:16-18. Print.

4. *Diarrhoeal Disease,* World Health Organization (WHO), 2013. Web 13 June 2014. http://www.who.int/mediacentre/factsheets/fs330/en/

5. Incropera, Frank P., and David P. DeWitt. *Fundamentals of Heat and Mass Transfer.* Hoboken: Wiley, 1996. Print.

6. Welty, J. et al. *Fundamentals of Momentum, Heat, and Mass Transfer.* Hoboken: Wiley, 2007. Print.

7. Burdock, TJ. et al. "A Dehydrogenase Activity Test for Monitoring the Growth of *Streptomyces Venezuelae* in a Nutrient Rich Medium". *J Bioprocess Biotechniq*, 1:101 (2010) doi:10.4172/2155-9821.1000101

8. Pandey, P.K., and M.L. Soupir, "Escherichia coli inactivation kinetics in anaerobic digestion of dairy manure under moderate, mesophilic and thermophilic temperatures." *AMB Express*, 1. (2011), Web 15 June 2013. *Science Direct.*

9. Popat, S. C.; Yates, M. V.; Deshusses, M. A., Kinetics of inactivation of indicator pathogens during thermophilic anaerobic digestion. *Wat. Res.*, **2010**, *44*, 5965-5972.